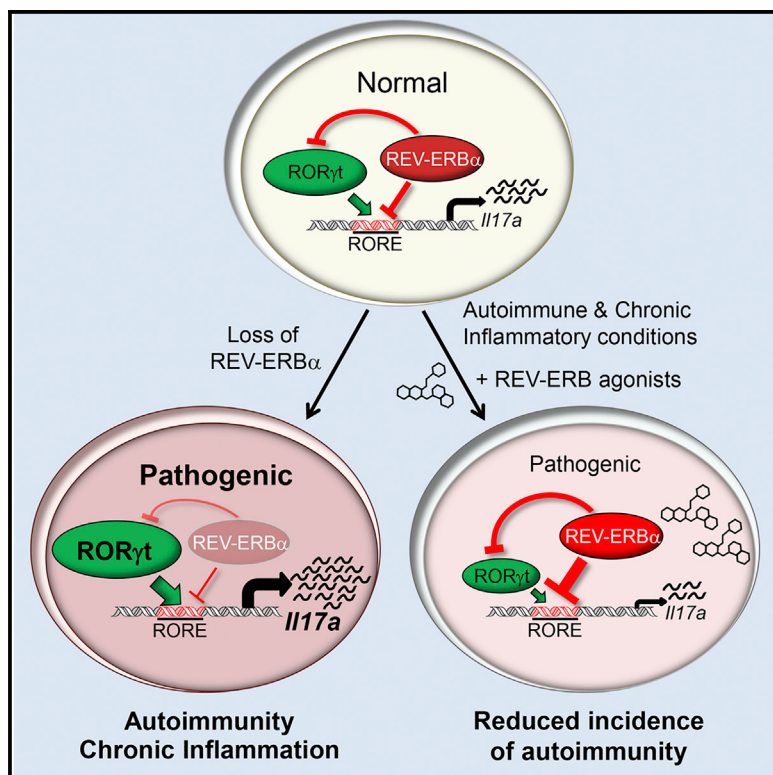


REV-ERB α Regulates T_H17 Cell Development and Autoimmunity

Graphical Abstract



Authors

Mohammed Amir, Sweena Chaudhari, Ran Wang, ..., Douglas J. Kojetin, Theodore M. Kamenecka, Laura A. Solt

Correspondence

Isolt@scripps.edu

In Brief

Roles for the circadian protein REV-ERB α have not been extensively explored in the immune system. Amir et al. demonstrate that REV-ERB α acts as a negative regulator of pro-inflammatory T_H17 cell development and function, and REV-ERB α ligands are efficacious in mouse models of autoimmunity.

Highlights

- REV-ERB α is upregulated in T_H17 cells
- REV-ERB α deficiency exacerbates T_H17-mediated diseases, including EAE and colitis
- REV-ERB α competes with ROR γ t to modulate T_H17-signature genes, including *Il17a*
- REV-ERB α -specific ligands suppress the development and progression of autoimmunity



REV-ERB α Regulates T_H17 Cell Development and Autoimmunity

Mohammed Amir,^{1,5} Sweena Chaudhari,^{1,5} Ran Wang,^{1,6} Sean Campbell,¹ Sarah A. Masure,^{1,2,3} Laura B. Chopp,^{1,7,8} Qun Lu,^{1,4} Jinsai Shang,³ Oliver B. Pelleter,¹ Yuanjun He,⁴ Christelle Doebelin,⁴ Michael D. Cameron,⁴ Douglas J. Kojetin,³ Theodore M. Kamenecka,⁴ and Laura A. Solt^{1,4,9,*}

¹Department of Immunology and Microbiology, The Scripps Research Institute, Jupiter, Florida 33458, USA

²Scripps Research, Skaggs Graduate School of Chemical and Biological Sciences, The Scripps Research Institute, La Jolla, California 92037, USA

³Department of Integrative Structural and Computational Biology, The Scripps Research Institute, Jupiter, Florida 33458, USA

⁴Department of Molecular Medicine, The Scripps Research Institute, Jupiter, Florida 33458, USA

⁵These authors contributed equally

⁶Present address: Inflammatory Disease Biology and Therapeutics Group, Mater Research Institute, The University of Queensland, Translational Research Institute, Brisbane, QLD 4102, Australia

⁷Present address: Laboratory of Immune Cell Biology, Center for Cancer Research, National Cancer Institute, NIH, Bethesda, Maryland, USA

⁸Present address: Immunology Graduate Group, University of Pennsylvania Medical School, Philadelphia, Pennsylvania, USA

⁹Lead contact

*Correspondence: lsolt@scripps.edu

<https://doi.org/10.1016/j.celrep.2018.11.101>

SUMMARY

ROR γ t is well recognized as the lineage-defining transcription factor for T helper 17 (T_H17) cell development. However, the cell-intrinsic mechanisms that negatively regulate T_H17 cell development and autoimmunity remain poorly understood. Here, we demonstrate that the transcriptional repressor REV-ERB α is exclusively expressed in T_H17 cells, competes with ROR γ t for their shared DNA consensus sequence, and negatively regulates T_H17 cell development via repression of genes traditionally characterized as ROR γ t dependent, including *Il17a*. Deletion of REV-ERB α enhanced T_H17-mediated pro-inflammatory cytokine expression, exacerbating experimental autoimmune encephalomyelitis (EAE) and colitis. Treatment with REV-ERB-specific synthetic ligands, which have similar phenotypic properties as ROR γ modulators, suppressed T_H17 cell development, was effective in colitis intervention studies, and significantly decreased the onset, severity, and relapse rate in several models of EAE without affecting thymic cellularity. Our results establish that REV-ERB α negatively regulates pro-inflammatory T_H17 responses *in vivo* and identifies the REV-ERBs as potential targets for the treatment of T_H17-mediated autoimmune diseases.

INTRODUCTION

T helper 17 (T_H17) cells are a subset of CD4 $^{+}$ T helper cells that preferentially secrete interleukin 17A (IL-17A), IL-17F, IL-21, and IL-22 and are important during tissue inflammation and

anti-microbial and anti-fungal immunity (McGeachy and Cua, 2008). Under homeostatic conditions, T_H17 cells have essential roles in protective immunity against extracellular pathogens at mucosal barriers (McGeachy and Cua, 2008). However, T_H17 cells have also been associated with the pathogenesis of several autoimmune diseases, including multiple sclerosis and psoriasis (Cho, 2008; Lees et al., 2011; Nair et al., 2009), suggesting that the failure of T_H17 cell homeostasis may give rise to disease. A significant amount of work has identified key factors that drive T_H17 cell development and pathogenicity. However, cell-intrinsic mechanisms that negatively regulate T_H17 cell development and associated inflammatory responses have received less attention. Therefore, a more comprehensive understanding of the factors that both positively and negatively regulate T_H17 cell development is necessary to better understand T_H17-mediated autoimmunity and would aid in the development of novel therapeutics to treat T_H17-mediated diseases.

A number of studies have identified key factors that drive T_H17 cell development and pathogenicity, including both the nuclear receptors retinoic-acid-receptor-related orphan receptor α and γ t (Ivanov et al., 2006; Yang et al., 2008). ROR γ t is considered the lineage-defining transcription factor regulating T_H17 cell development, and a considerable amount of research has elucidated genomic functions of ROR γ t. Two other members of the nuclear receptor superfamily, REV-ERB α (NR1D1) and REV-ERB β (NR1D2), are often co-expressed in the same tissues as the RORs and bind the same DNA response elements, resulting in mutual cross-talk and co-regulation of their shared target genes (Kojetin and Burris, 2014). Outside of the immune system, the RORs and the REV-ERBs modulate a number of physiological processes but are best known for their roles in the regulation of the circadian rhythm, lipid, and glucose metabolic processes. The REV-ERBs are unique within the nuclear receptor superfamily in that they lack the carboxy-terminal tail of their ligand-binding domain (LBD) called the activation function 2 region (AF-2, helix 12), which is required for coactivator recognition. Thus, in



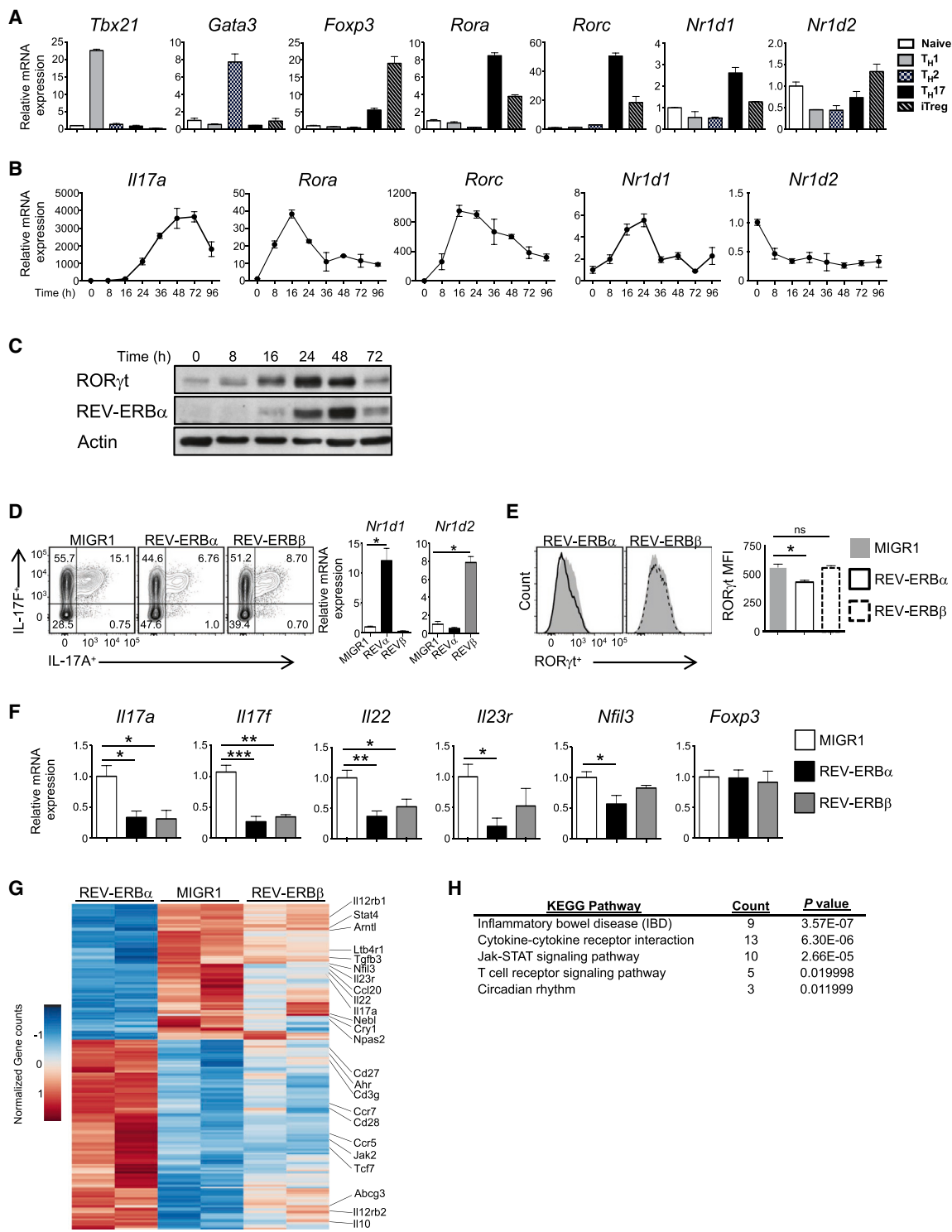


Figure 1. The REV-ERBs Inhibit T_H17 Cell Development

(A) Quantitative real-time PCR analysis of T helper cell lineage-specific transcription factors T-bet (*Tbx21*), Gata3, Foxp3, ROR α (*Rora*), ROR γ t (*Rorc*), REV-ERB α (*Nr1d1*), and REV-ERB β (*Nr1d2*) under T_H1, T_H2, T_H17, and inducible T regulatory cell (iTreg) conditions at 48 hr after T cell-activation compared to naive CD4⁺ T cells (n = 3).

(B) Quantitative real-time PCR of *II17a*, *Rora*, *Rorc*, *Nr1d1*, and *Nr1d2* expression during T_H17 cell differentiation. Data represent mean ± SEM (n = 3).

(C) Immunoblot analysis of REV-ERB α and ROR γ t expression during T_H17 cell differentiation (n = 4).

(legend continued on next page)

contrast to the RORs, which are constitutive activators of transcription, the REV-ERBs are transcriptional repressors (Kojetin and Burris, 2014). Collectively, the balance of expression of the RORs and REV-ERBs is critical for dynamic regulation of their target genes (Kojetin and Burris, 2014). While much is known about ROR γ t-mediated regulation of T H 17 cell development and function, little is known about the role of the REV-ERBs in T cell effector functions, specifically pro-inflammatory T H 17 cell effector functions and autoimmunity.

Most members of the nuclear receptor superfamily are ligand-regulated transcription factors and represent attractive therapeutic targets, including ROR γ t. After the initial identification of several synthetic ROR γ modulators, including SR1001 and digoxin (Huh et al., 2011; Solt et al., 2011), countless other ROR γ ligands have been identified, demonstrating the tractability of ROR γ t-targeted treatment of T H 17-mediated autoimmunity (Bronner et al., 2017). The REV-ERBs are also ligand-regulated transcription factors, and the porphyrin heme was identified as the endogenous ligand for both REV-ERB α and REV-ERB β (Raghuram et al., 2007; Yin et al., 2007). We and others have identified and characterized synthetic ligands that modulate the activity of the REV-ERBs both *in vitro* and *in vivo* (Banerjee et al., 2014; Kojetin et al., 2011; Solt et al., 2012). We previously synthesized and characterized SR9009 and SR9011 for their activity and specificity to target the REV-ERBs, demonstrating that *in vivo* pharmacological modulation of REV-ERB activity affected REV-ERB-mediated processes, including regulation of the circadian rhythm, glucose, and lipid metabolic processes (Solt et al., 2012). Despite the well-documented overlap in genetic programs between the RORs and REV-ERBs in tissues outside of the immune system (Kojetin and Burris, 2014), the role for the REV-ERBs in T H 17 cell development is still poorly understood. Furthermore, given the massive pharmaceutical effort focused on developing potent ROR γ -modulators, small-molecule modulators of REV-ERB activity could represent a novel therapeutic target for the treatment of T H 17-mediated autoimmunity.

While REV-ERB α was previously demonstrated to diurnally regulate T H 17 cell frequencies *in vivo* (Yu et al., 2013), its function in the context of pro-inflammatory settings and autoimmunity remains poorly defined. Here, we show that REV-ERB α is expressed during T H 17 cell development and its presence is required for dampening T H 17-mediated pro-inflammatory cytokine expression. Overexpression of REV-ERB α suppressed T H 17 cell development, whereas genetic deletion of REV-ERB α resulted in enhanced T H 17 cell development *in vitro* and exacerbated autoimmune responses *in vivo*. We found that while REV-

ERB α directly repressed *Nfil3* (Yu et al., 2013), it also competed with ROR γ t for binding at the *Il17a* promoter and CNS-5 enhancer region. We also discovered that REV-ERB α binds within the *Rorc* promoter region, suggesting potential cross-talk and autoregulation among these receptors for controlling T H 17 cytokine expression. Finally, the use of REV-ERB-specific small molecules that we developed suppressed T H 17 cell development *in vitro* and the development of T H 17-mediated autoimmunity *in vivo* and was effective when used in a “treatment mode” in several models of autoimmunity and chronic inflammation. However, unlike ROR γ modulators, REV-ERB modulators did not have effects on the thymus. Collectively, our data suggest that REV-ERB α functions outside of its classical role as a core member of the circadian clock under pro-inflammatory conditions and importantly, is a key cell-intrinsic negative regulator of T H 17 cell pro-inflammatory immune responses.

RESULTS

REV-ERB α Is Upregulated in T H 17 Cells

To determine whether the REV-ERBs were expressed during CD4 $^+$ T helper cell development, we differentiated naive CD4 $^+$ T cells into T H 1, T H 2, T H 17, or inducible T regulatory cells (iTregs). REV-ERB α was upregulated at the mRNA level in T H 17 cells, whereas REV-ERB β was not (Figure 1A). We next performed a kinetic analysis and discovered the expression pattern of REV-ERB α was similar to that of the RORs, whereas REV-ERB β was downregulated during development (Figures 1B and 1C). The similar expression pattern profiles between the RORs and REV-ERB α are consistent with other published data demonstrating that the RORs drive REV-ERB α expression through conserved ROR response elements (ROREs) within its promoter region (Raspè et al., 2002; Takeda et al., 2012). Furthermore, the disconnect in expression between REV-ERB α and REV-ERB β is unique given that the REV-ERBs typically have overlapping tissue expression patterns (Kojetin and Burris, 2014), suggesting that REV-ERB α may play a role in the regulation of T H 17 cell development.

The REV-ERBs Repress T H 17 Cell Development

To better assess the function of the REV-ERBs in T H 17 cells, we retrovirally overexpressed an empty vector (MIGR1), REV-ERB α , or REV-ERB β in T H 17 cells. Although the expression of both REV-ERBs inhibited IL-17A and IL-17F expression, REV-ERB α was more potent (Figure 1D). The inhibitory effect of the REV-ERBs appeared to be T H 17-cell specific because it did not affect the expression of Foxp3 in iTreg cells (Figure S1A). Interestingly,

(D) FACS analysis of IL-17A and IL-17F expression in T H 17 cells transduced with empty vector (MIGR1), REV-ERB α , or REV-ERB β . Cells were gated on live, GFP $^+$ cells. Quantitative real-time PCR analysis of REV-ERB α and REV-ERB β expression from sorted GFP $^+$ T H 17 cells transduced with MIGR1, REV-ERB α , or REV-ERB β ($n = 4$).

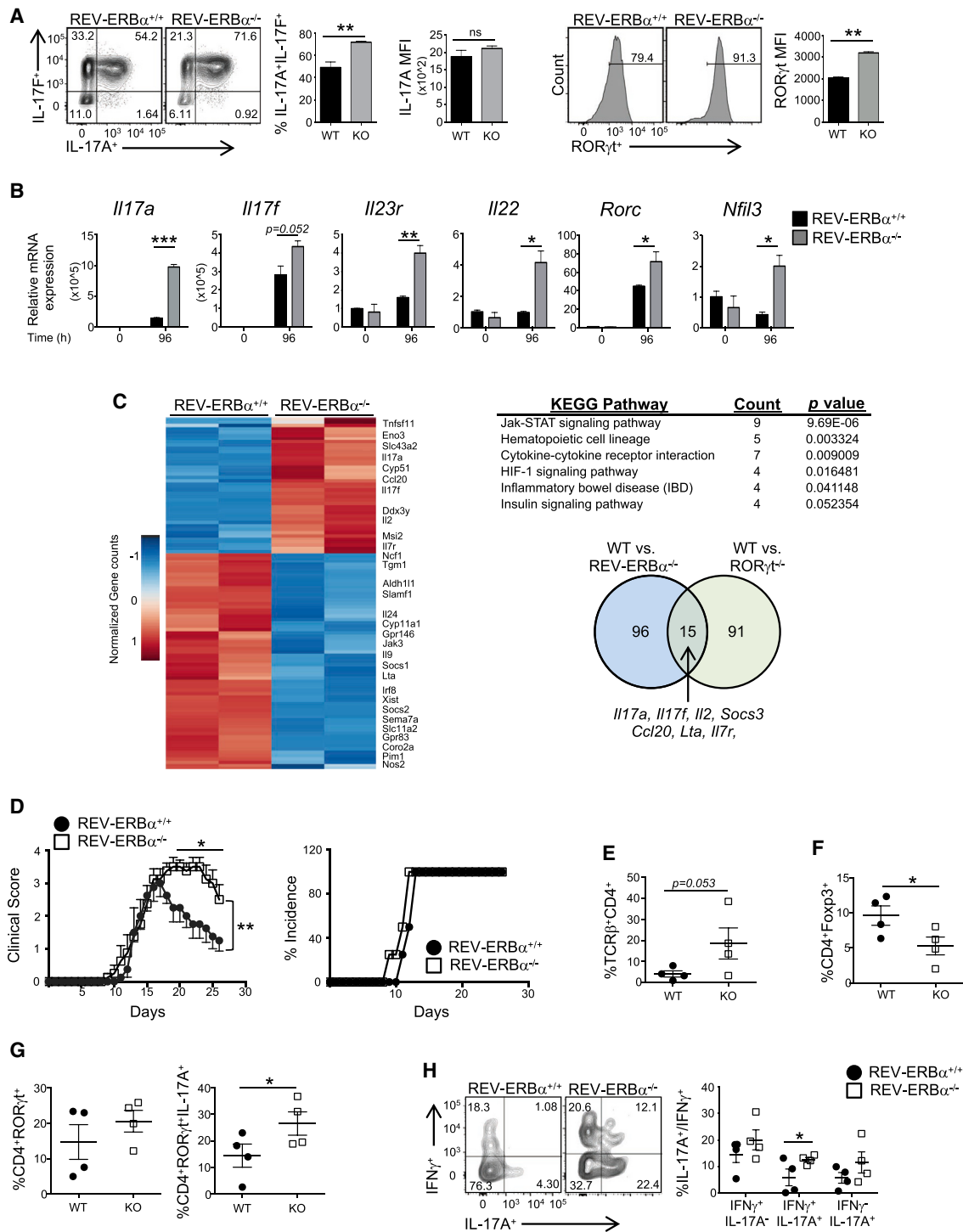
(E) FACS analysis of ROR γ t expression from T cell cultures shown in (D). Graph (right) indicates median fluorescent intensity (MFI) of ROR γ t expression in the FACS plots.

(F) Quantitative real-time PCR of sorted GFP $^+$ cells from (D) ($n = 3$).

(G) Heatmap of differentially expressed genes in T H 17 cells (false discovery rate [FDR], <0.05).

(H) KEGG pathway analysis of genes differentially expressed between MIGR1-, REV-ERB α -, and REV-ERB β -overexpressing T H 17 cells.

β -actin was used as the internal control for quantitative real-time PCR. * $p < 0.05$, ** $p < 0.01$, and *** $p < 0.001$ determined using Student's t test. ns, not significant ($p > 0.05$).

**Figure 2. Loss of REV-ERB α Leads To Increased T_H17-Mediated Autoimmunity**

(A) FACS analysis from T_H17 cultures derived from REV-ERB $\alpha^{+/+}$ (WT) and REV-ERB $\alpha^{-/-}$ (KO) mice. Graphs indicate percent IL-17A⁺IL-17F⁺ cells (top) and MFI of ROR γ t expression in the FACS plots (bottom) ($n = 4$).

(B) Quantitative real-time PCR of T_H17-mediated cytokines in T_H17 cell cultures from WT and KO mice. β -actin was used as the internal control ($n = 3$).

(C) Heatmap of differentially expressed genes between WT and KO T_H17 cells. KEGG pathway analysis of genes differentially expressed between WT and KO T_H17 cells. Venn diagram depicting the numbers of unique and shared genes differentially regulated in WT/KO and WT/ROR γ t^{-/-} T_H17 cells (FDR, <0.05).

(D) Clinical EAE scores (left) and disease incidence (right) from WT and KO mice subjected to MOG-induced EAE.

(legend continued on next page)

overexpression of REV-ERB α but not REV-ERB β resulted in decreased ROR γ t expression in transduced T H 17 cells (Figure 1E). Quantitative real-time PCR analysis on sorted transduced samples demonstrated a significant decrease in expression of T H 17-cell signature genes and *Nfil3* (Figure 1F). Although the REV-ERB α -mediated repression on *Nfil3* was consistent with previously published work (Yu et al., 2013), the reduction in T H 17-cell signature genes was not. Given the striking effects of REV-ERB α on *Nfil3* and T H 17-mediated gene expression, we wanted to assess how *Nfil3* fit into this paradigm. We retrovirally overexpressed or knocked down *Nfil3* in T H 17 cells and found each to have little effect on IL-17A expression (Figures S1B and S1C). This is consistent with a prior study that demonstrated similar results (Ciofani et al., 2012). Collectively, our data suggest that REV-ERB α may be playing a more direct role in T H 17 cell development than previously identified.

To better understand the transcriptional programs dictated by the REV-ERBs during T H 17 cell development, we performed RNA sequencing on T H 17 cells transduced with an empty vector, REV-ERB α , or REV-ERB β retrovirus. Consistent with our quantitative real-time PCR data, REV-ERB α transduced cells repressed a number of T H 17 cell signature genes, including the “core” ROR γ t target genes *I17a*, *I17f*, *Tgfb3*, *Ccl20*, and *Ltb4r1* (Ciofani et al., 2012), relative to MIGR1 controls (adjusted p value [p. adj.] < 0.05) (Figure 1G and Table S1). KEGG pathway analysis indicated that REV-ERB α differentially regulated genes associated with inflammatory bowel disease (IBD), which is consistent with the involvement of T H 17 cells in the pathogenesis of IBD (Harbour et al., 2015; Jostins et al., 2012; Lee et al., 2009), cytokine-cytokine receptor interactions, Jak-STAT signaling pathways, T cell receptor signaling, and the circadian rhythm (Figure 1H). Overexpression of REV-ERB β had a modest effect on global T H 17 cell gene changes relative to REV-ERB α . These data suggest that REV-ERB α is a potent repressor of the T H 17 cell genetic program.

Cell Intrinsic Role for REV-ERB α in Restraining T H 17 Cell Development and Inflammatory Responses *In Vivo*

We next used REV-ERB $\alpha^{-/-}$ mice (Chomez et al., 2000) to explore the endogenous role of REV-ERB α in T H 17 cell development. Immune phenotyping revealed no overt differences between REV-ERB $\alpha^{+/+}$ (wild-type [WT]) and REV-ERB $\alpha^{-/-}$ (KO) mice (Figures S2A–S2C). We differentiated WT and KO naive CD4 $^+$ T cells under T H 1-, T H 2-, T H 17-, or iTreg-polarizing conditions and observed a significant increase in the frequency of IL-17A $^+$ IL-17F $^+$ cells and the expression of ROR γ t in T H 17 cells (Figure 2A). Similar results were observed across various T H 17 cell culture conditions, including pathogenic T H 17 conditions (Lee et al., 2012; Peters et al., 2011), with little to no effect on

the development of T H 1 and T H 2 cells (Figures S3A–S3C). Although a prior study found that REV-ERB α deficiency resulted in decreased IL-17A production *in vitro*, differences in the culture conditions, protocols, and mouse strains could account for the different outcomes (Yu et al., 2013). However, REV-ERB α deficiency resulted in reduced expression of Foxp3 and increased expression of ROR γ t in iTreg cultures (Figure S3D). Because overexpression of REV-ERB α did not affect iTreg development *in vitro*, these results suggested this was possibly through REV-ERB α -dependent effects on ROR γ t expression. REV-ERB α deficiency also increased the expression of T H 17 signature genes as well as *Nfil3* (Figure 2B), consistent with a direct relief of repression expected when a transcriptional repressor is deleted (Cho et al., 2012; Everett and Lazar, 2014). Finally, we performed RNA sequencing to examine the global transcriptional effects of REV-ERB α deficiency on T H 17 cell development. Similar to our overexpression studies (Figure 1), REV-ERB α -deficient T H 17 cells differentially expressed numerous T H 17 cell signature genes, including *I17a*, *I17f*, *Ccl20*, and *Lta*, relative to WT control cells (p. adj. < 0.05) and regulated similar pathways identified by KEGG pathway analysis (Figure 2C and Table S2). Because REV-ERB α and ROR γ bind to the same DNA response elements, we compared our data to previously published data that assessed ROR γ knockout T H 17 cells (Ciofani et al., 2012). Although we observed only a small overlap in genes, most of the overlapping genes were the core ROR γ t target genes (Ciofani et al., 2012) (Figure 2C). These data indicate that REV-ERB α affects T H 17 cell development through several mechanisms, including ROR γ t-dependent T H 17 cell cytokine expression.

To determine whether REV-ERB α influenced T H 17-mediated autoimmunity, we immunized WT and KO mice with a myelin oligodendrocyte glycoprotein peptide (MOG_{35–55}) to induce experimental autoimmune encephalomyelitis (EAE), a mouse model of multiple sclerosis. Signs of disease were exacerbated, and the onset of disease was slightly earlier in KO mice compared to WT littermate controls (Figure 2D). We observed an increased frequency of CD4 $^+$ T cells infiltrating the CNS of the KO mice at the peak of disease (Figure 2E). Of the infiltrating CD4 $^+$ T cells in the CNS, the overall frequency of ROR γ t $^+$ cells was elevated (Figure 2G). This correlated with the increased expression of IL-17A $^+$ T cells in the CNS, whereas the percent of anti-inflammatory Foxp3 $^+$ Tregs was significantly decreased (Figures 2F and 2G). Because T H 17 cells can give rise to T H 1-like cells that produce IFN γ , and acquisition of IFN γ has been linked to their pathogenicity in several models of chronic disease (Ghoreschi et al., 2010; Hirota et al., 2011; Lee et al., 2009), we assessed the frequency of IL-17A $^+$, IL-17A $^+$ IFN γ $^+$, and IFN γ $^+$ T cells in the CNS (Figure 2H). There was a significant increase in the IL-17A $^+$ IFN γ $^+$ population in KO mice compared to WT

(E and F) Graphs summarizing the frequency of TCR β $^+$ CD4 $^+$ cells (E) and Foxp3 $^+$ cells in the CNS of mice (F).

(G) Graph representing FACS analysis of ROR γ t expression (left) and total IL-17A expression in ROR γ t $^+$ cells (right) in the TCR β $^+$ CD4 $^+$ cells in the CNS of WT and KO mice.

(H) FACS analysis and graph depicting the frequency of IL-17A $^+$ IFN γ $^-$, IL-17A $^+$ IFN γ $^+$, and IL-17A $^+$ IFN γ $^+$ cells in the CNS of WT and KO mice.

Cells were gated on live, CD45 $^+$ TCR β $^+$ CD4 $^+$ cells. Each symbol represents an individual mouse (n = 4/group). Data represent mean \pm SEM and are representative of two separate independent experiments generating similar results. Two-way ANOVA (clinical score) and Student's t tests were performed for statistical analysis.
*p < 0.05, **p < 0.01, ***p < 0.001.

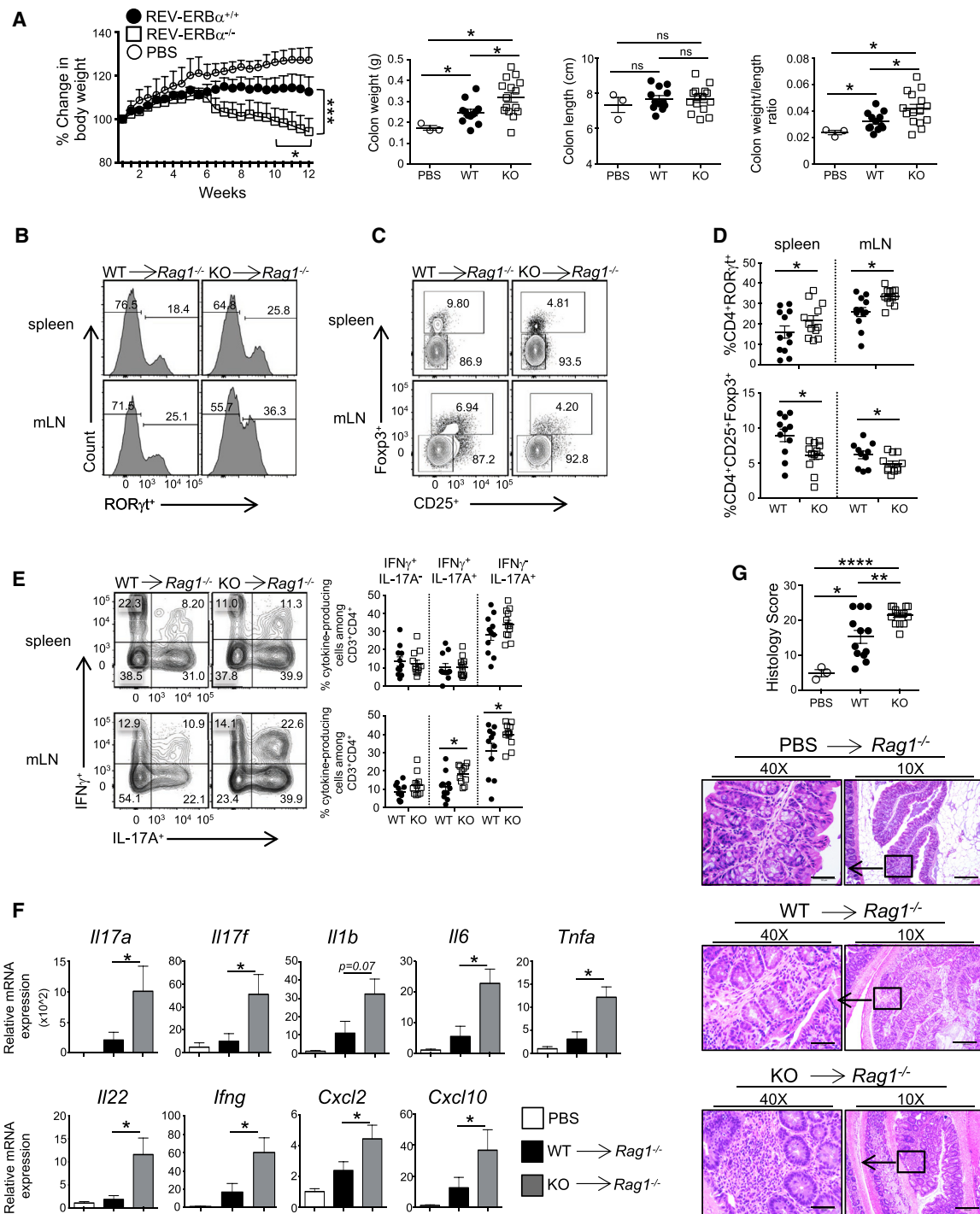


Figure 3. Loss of REV-ERB α in T Cells Exacerbates Colitis

(A) Percent change in body weight, colon weights, colon lengths, and colon weight versus colon length ratios of $Rag1^{-/-}$ recipient mice over 12 weeks post-adoptive transfer of WT, KO, or control (no cells, PBS) T cells.

(B-D) FACS plots demonstrating frequencies of (B and D) ROR γ t $^+$ and (C and D) CD25 $^+$ Foxp3 $^+$ cells in the spleens and mesenteric lymph nodes (mLN) of recipient mice at the termination of the experiment.

(E) FACS analysis and frequencies of IL-17A $^+$ IFN γ $^-$, IL-17A $^+$ IFN γ $^+$, and IL-17A $^-$ IFN γ $^+$ cells in the spleens and mLNs of recipient mice. Cells were gated on live, CD45 $^+$ CD3 $^+$ CD4 $^+$ cells.

(F) Quantitative real-time PCR analysis of cytokines and chemokines expressed in the proximal colon from $Rag1^{-/-}$ mice receiving PBS, WT, or KO CD4 $^+$ T cells. 18s was used as the internal control.

(legend continued on next page)

controls. These results indicated that the loss of REV-ERB α leads to increased pro-inflammatory responses *in vivo*.

REV-ERB α Deficiency Exacerbates the Development of Colitis

To determine the T cell-specific effects of REV-ERB α *in vivo*, we sorted naive CD4 $^+$ T cells from WT and KO mice and adoptively transferred them into *Rag1* $^{-/-}$ recipients to track the development of colitis, which is another T H 17-driven inflammatory disorder (Harbour et al., 2015; Lee et al., 2009) by using PBS-sham injections as a control. The transfer of KO cells resulted in more severe weight loss and intestinal inflammation than WT cells (Figure 3A). Mice receiving KO T cells had an increased frequency of ROR γ T $^+$ T H 17 cells and decreased frequency of Foxp3 $^+$ Tregs relative to WT recipient mice in spleens and mesenteric lymph nodes (mLNs) (Figures 3B–3D). Mice receiving KO T cells also had an increased frequency of IL-17A $^+$ and pathogenic IL-17A $^+$ IFN γ $^+$ cells (Figure 3E). The expression of T H 17-associated cytokines (*Il17a*, *Il17f*, and *Il22*), pro-inflammatory cytokines (*Il1b*, *Il6*, *Tnfa*, and *Ifng*), and genes activated downstream of IL-17A and IL-17F and IL-22 signaling (*Cxcl2* and *Cxcl10*) were increased at the mRNA level in whole-tissue homogenates of the proximal colons of mice receiving KO T cells (Figure 3F). Finally, histological analysis of the proximal colons demonstrated increased cellular infiltration, broadening of the crypts, and epithelial hyperplasia in mice receiving KO T cells compared to WT controls (Figure 3G). Similar results were observed in the distal colon of the recipient mice (data not shown). These results indicate that the loss of REV-ERB α promotes T cell-mediated colitis, leading to increased frequencies of pro-inflammatory T H 17 and IFN γ -producing T H 17 cells, reinforcing the role of REV-ERB α as a negative regulator of pro-inflammatory T H 17 responses.

REV-ERB α Competes with ROR γ t To Repress T H 17 Cell Development

We next sought to delineate the molecular mechanisms underlying REV-ERB α -dependent repression of T H 17 cell development. Because the RORs and REV-ERBs bind to the same genomic DNA response element sequence, an RGGTCA half-site preceded by a 5'-AT-rich region (RORE and/or REV-ERB response element [RevRE]), we wanted to determine if REV-ERB α could bind and repress within the *Il17a* locus, a known ROR γ t target gene (Figure 4A). Cotransfection assays in HEK293 cells using an *Il17a*+CNS5 luciferase reporter construct (Zhang et al., 2008) demonstrated that REV-ERB α repressed *Il17a*+CNS5-luciferase driven activity in a concentration-dependent manner (Figure 4B). This effect was dependent on the ability of REV-ERB α to bind DNA because deletion of its DNA-binding domain (DBD) had no effect on luciferase activity, whereas the REV-ERB α DBD alone also dose-dependently inhibited *Il17a*+CNS5-luciferase driven activity. We next performed competition

experiments in HEK293 cells to determine if REV-ERB α competes with ROR γ t at their shared RORE and/or RevRE in the *Il17a* promoter and enhancer region. Consistent with Figure 4B, REV-ERB α competed with ROR γ t for its shared RORE and/or RevRE in a concentration-dependent manner to regulate *Il17a*+CNS5-luciferase driven activity (Figure 4C). The reduced repression observed with the DBD construct compared with the full-length REV-ERB α is likely due to its inability to recruit corepressor proteins, such as NCoR, via its LBD for active repression (Yin et al., 2010). Finally, in EL4 mouse T cell thymoma cells that endogenously expresses ROR γ t, we found that REV-ERB α competes with endogenous ROR γ t using the *Il17a*+CNS5-luciferase reporter (Figure 4D).

To establish whether REV-ERB α modulates ROR γ t-mediated IL-17A expression in a DBD-dependent manner in T H 17 cells, we retrovirally overexpressed empty vector, full-length REV-ERB α , REV-ERB α DBD, or REV-ERB α ΔDBD in T H 17 cells and assessed IL-17A expression by flow cytometry. Both FL and REV-ERB α DBD significantly inhibited IL-17A protein expression, whereas IL-17A expression in the REV-ERB α ΔDBD condition was similar to the empty vector control (Figure 4E). Finally, using an anti-REV-ERB α antibody (Cho et al., 2012), chromatin immunoprecipitation (ChIP) experiments in T H 17 cells indicated that endogenous REV-ERB α was bound within the promoter and CNS5 region of the *Il17a* gene, suggesting that regulation of *Il17a* transcription is direct (Yang et al., 2008) (Figure 4F). We also observed REV-ERB α bound within the upstream promoter region of *Rorc* (Mongrain et al., 2008) and *Nfil3* (Yu et al., 2013), which is consistent with published results; *Cry1* (Cho et al., 2012) and *Hprt* were used as positive and negative controls, respectively. These data indicate that REV-ERB α negatively regulates T H 17 cell development by competing with ROR γ t at the RORE and/or RevRE sites, which includes the *Il17a* locus. Furthermore, an additional layer of regulation may occur through REV-ERB α -mediated repression of ROR γ t.

REV-ERB α -Specific Small Molecules Suppress T H 17-Cell Development

We previously developed and characterized SR9009, a proof-of-concept REV-ERB-specific synthetic ligand that demonstrated that the REV-ERBs could be pharmacologically targeted *in vivo* (Solt et al., 2012). Our efforts to improve SR9009 led to our identification of SR12418, which binds to both receptors in a time-resolved fluorescence resonance energy transfer (TR-FRET) biochemical assay and is more potent at REV-ERB α (half maximal inhibitory concentration [IC_{50}] = 68 nM) and REV-ERB β (IC_{50} = 119 nM) in a *Bm1*-luciferase reporter assay than SR9009 (Figures S4A–S4C, S5A, and S5B) (Noel et al., 2012). SR12418 demonstrated significantly improved plasma exposure relative to SR9009 (Solt et al., 2012), was more effective at inhibiting IL-17A expression in EL4 cells, demonstrated specificity at the REV-ERBs, and did not exhibit activity at any

(G) Histology scores from colon and representative hematoxylin and eosin stained proximal colon sections from *Rag1* $^{-/-}$ recipient mice 12 weeks after transfer of naive CD4 $^+$ T cells. ($\times 10$ magnification, scale bars represent 200 μ m; $\times 40$ magnification, scale bars represent 50 μ m) (n = 13 for WT, n = 15 for KO, and n = 3 for PBS).

Data represent mean \pm SEM. Two-way ANOVA (body weight) and Student's t tests were performed for statistical analysis. *p < 0.05, **p < 0.001, ***p < 0.001, ****p < 0.0001.

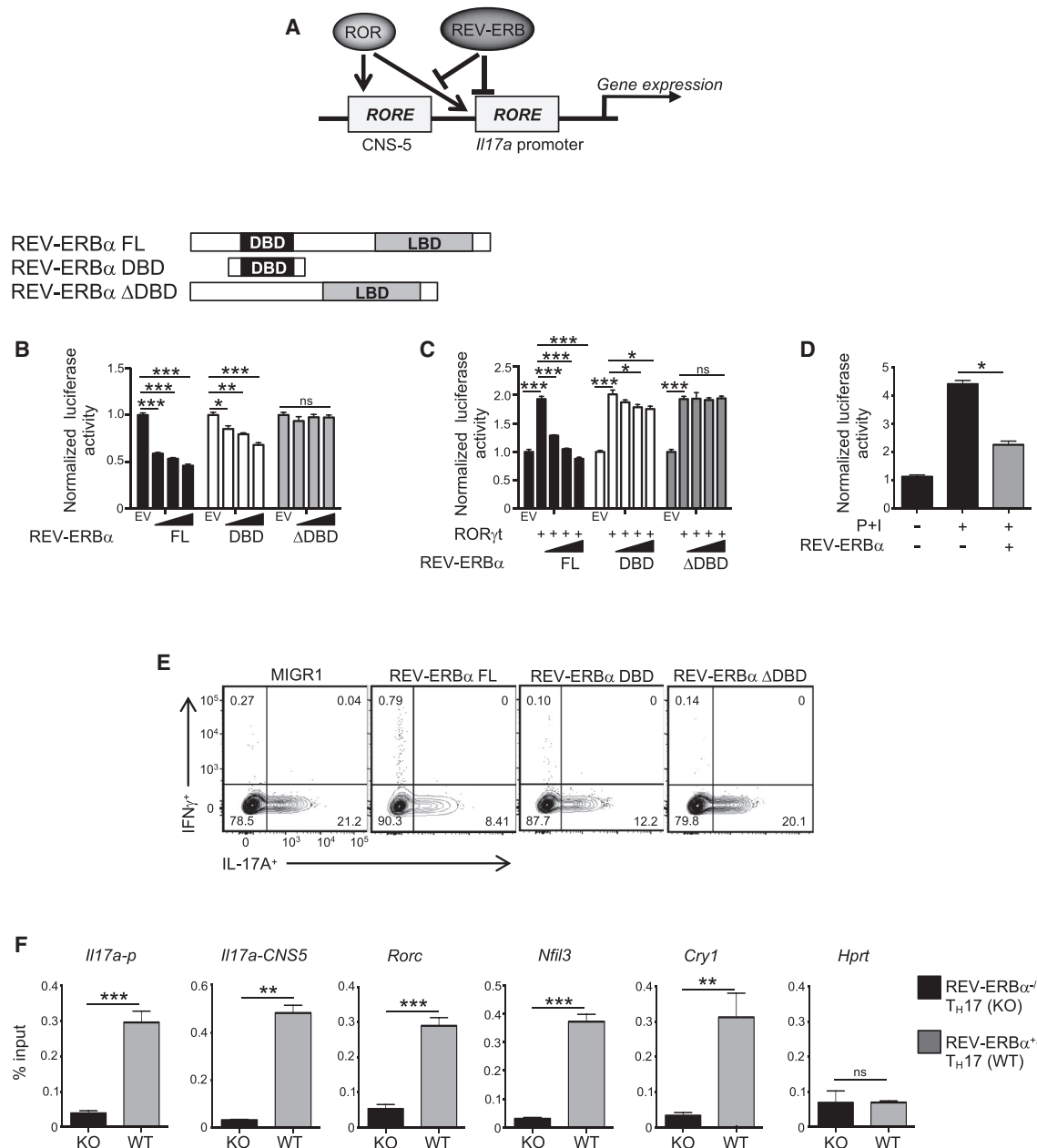


Figure 4. REV-ERB α Competes with ROR γ t To Repress T_H17 Cell Development

(A) Schematic demonstrating REV-ERB α and ROR γ t competition for the IL17a locus.

(B) Schematic of REV-ERB α constructs. Cotransfection assays in HEK293 cells demonstrating full-length (FL) and REV-ERB α DBD dose-dependently suppresses IL17a + CNS5 luciferase activity. EV refers to empty vector. (n = 5).

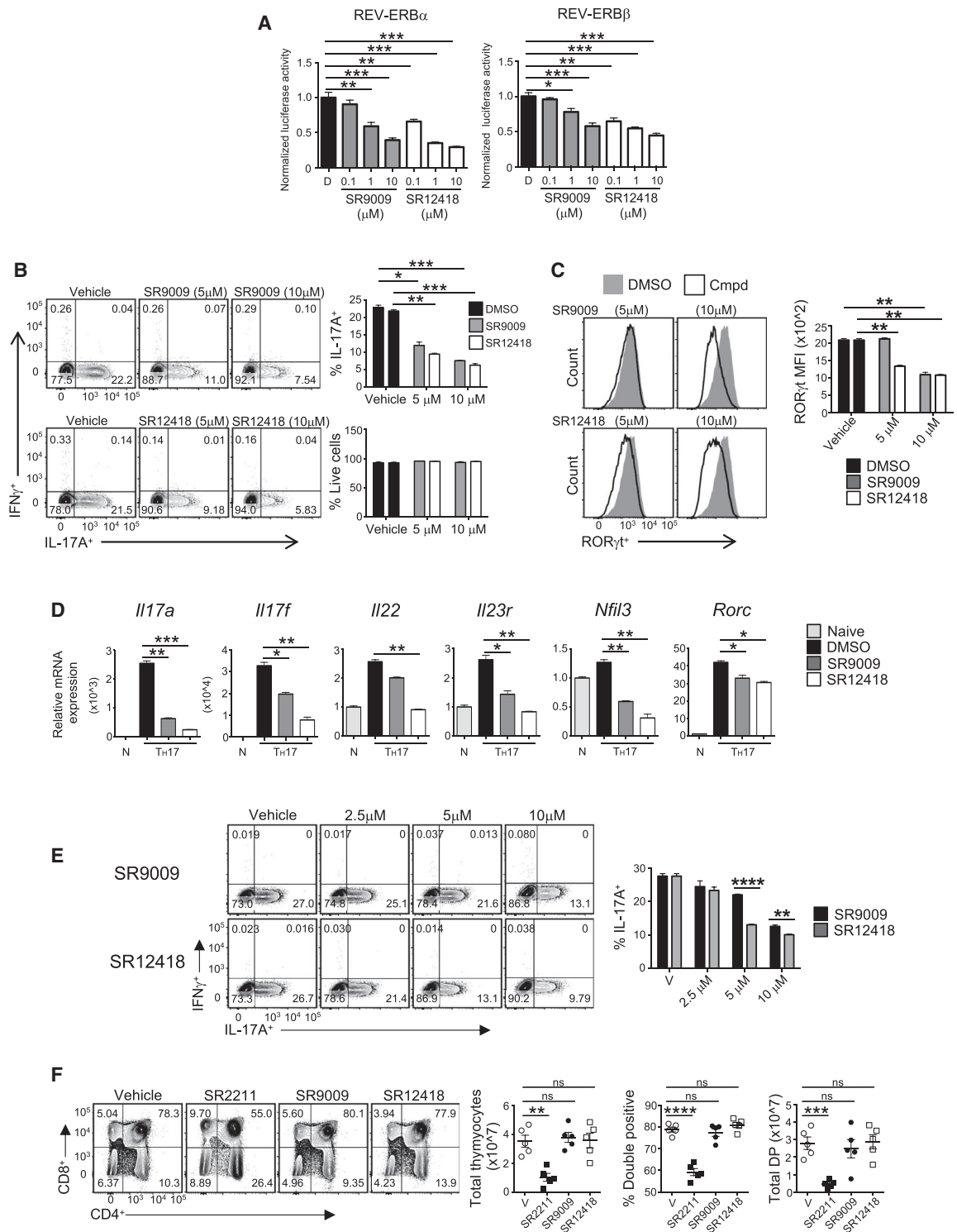
(C) Cotransfection assay in HEK293 cells demonstrating that FL and REV-ERB α DBD competes with ROR γ t binding at the IL17a + CNS5 RORE. The concentration of ROR γ t was constant in all conditions labeled with a (+). (n = 5).

(D) Cotransfection assay in EL4 cells demonstrating REV-ERB α competes with endogenous ROR γ t binding at the IL17a + CNS5 RORE. P+I indicates 18-hr stimulation with phorbol 12-myristate 13-acetate (PMA) and ionomycin (n = 4).

(E) FACS analysis of IL-17A and IFN γ expression in T_H17 cells transduced with MIGR1, FL REV-ERB α , REV-ERB α DBD, or REV-ERB α ΔDBD. Cells were gated on live, GFP⁺ cells (n = 4).

(F) ChIP-qPCR of REV-ERB α binding at various sites in KO and WT T_H17 cells collected on day 3. (IL17a-p, IL17a promoter).

Data represent mean \pm SEM (n = 4). *p < 0.05, **p < 0.01, ***p < 0.001 determined using Student's t test. ns, not significant (p > 0.05).

**Figure 5. REV-ERB α -Specific Small Molecules Suppress T H 17 Cell Development and Function**

(A) Cotransfection assay in HEK293 cells using FL REV-ERB α , REV-ERB β , and the *Il17a* + CNS5 luciferase reporter. Graphs demonstrate that SR9009 and SR12418 dose-dependently drive REV-ERB-mediated repression of *Il17a* + CNS5 luciferase activity. Data represent mean \pm SEM (n = 4).

(B) Mouse CD4 $^{+}$ T cells were differentiated under T H 17 polarizing conditions and treated with vehicle (DMSO), SR9009, or SR12418. IL-17A and IFN γ expression were analyzed by flow cytometry. Graphs indicate percent IL-17A $^{+}$ cells and frequency of live cells in cultures with compound treatment (n = 3).

(C) FACS analysis and graphs depicting MFI of ROR γ t expression in T H 17 cultures treated with SR9009 and SR12418.

(legend continued on next page)

other nuclear receptors (Figures S5C–S5F) (Solt et al., 2012). SR12418 also showed minimal off-target activity in a CEREP (Eurofins Scientific) panel screen of 84 G-protein coupled receptors, ion channels, and transporters (data not shown). Both SR9009 and SR12418 dose-dependently inhibited IL17a luciferase activity at REV-ERB α and REV-ERB β and inhibited $\text{T}_{\text{H}}17$ cell differentiation without affecting viability or other T helper populations (Figures 5A, 5B, S6A, and S6B). Expression of ROR γ t was also downregulated in drug-treated conditions relative to vehicle control (Figure 5C). Quantitative real-time PCR analysis demonstrated that SR9009 and SR12418 potently repressed $\text{T}_{\text{H}}17$ -mediated gene expression and *Nfil3*, which is consistent with REV-ERB α acting as a repressor at RORE and/or RevRE sites (Figure 5D). To establish whether REV-ERB-selective small molecules could override potent ROR γ t-driven $\text{T}_{\text{H}}17$ differentiation, we retrovirally transduced naive CD4 $^{+}$ T cells with ROR γ t cultured under $\text{T}_{\text{H}}17$ -polarizing conditions and treated the cells with SR9009, SR12418, or vehicle control. Despite the potent and sustained ectopic ROR γ t expression, REV-ERB-selective small molecules were able to repress ROR γ t-mediated IL-17A expression (Figure 5E). These data indicate that REV-ERB-selective small molecules can target the IL-17A pathway *in vitro* and override a potent ROR γ t stimulus.

Currently, ROR γ modulators are being developed for the treatment of autoimmunity (Guo et al., 2016). However, ROR γ t is required for thymocyte survival (Kurebayashi et al., 2000; Sun et al., 2000), and one drawback of treatment with ROR γ modulators is thymocyte apoptosis (Chang et al., 2014; Guo et al., 2016). To determine if REV-ERB ligands induced a similar phenotype, we treated C57BL/6 mice for 3 days with SR2211 (a potent ROR γ inverse agonist (Kumar et al., 2012) (20 mg/kg, i.p., b.i.d.), SR9009 (100 mg/kg, intraperitoneal [i.p.], twice a day [b.i.d.]), SR12418 (50 mg/kg, i.p., b.i.d), or vehicle control. Although mice treated with SR2211 demonstrated reduced thymic cellularity, specifically in the double-positive stage, treatment with SR9009 or SR12418 did not display significant defects relative to vehicle control. (Figure 5F). *Rorc*^{fl/fl} and *Rorc*^{fl/fl} × CD4 Cre mice were also analyzed as controls, and consistent with published reports, deletion of ROR γ in the thymus leads to reduced cellularity and apoptosis in the double-positive stage (Kurebayashi et al., 2000; Sun et al., 2000). (Figure S6C). Thus, ROR γ inverse agonists, such as SR2211, largely phenocopy the thymocyte apoptosis observed in ROR γ knockout mice, whereas REV-ERB synthetic ligands do not.

REV-ERB-Selective Small Molecules Suppress $\text{T}_{\text{H}}17$ -Mediated Autoimmunity *In Vivo*

As proof of concept, we tested whether pharmacologically targeting the REV-ERBs *in vivo* would affect autoimmune disease course by immunizing C57BL/6 mice to induce EAE. Due to its

superior pharmacological profile over SR9009, we focused on SR12418, which was administered daily (50 mg/kg, b.i.d.) versus vehicle control following immunization. Mice treated with SR12418 showed delayed onset and severity of disease compared to the vehicle-control-treated group (Figure 6A). The incidence of disease was greatly diminished in the SR12418 treated group, with approximately 20% of mice developing overt signs of disease compared to 90% of vehicle-control mice. SR12418 treatment did not demonstrate overt signs of toxicity, as the weight of the animals remained relatively constant throughout the experiment. Evaluation of liver demonstrated that SR12418 did not appear to significantly perturb the circadian rhythm in other tissues evaluated (Figure S7A). Evaluation of the draining LNs and CNS indicated a reduction in the frequency and number of CD3 $^{+}$ CD4 $^{+}$ T cells at the peak of disease (Figure 6B). Intracellular fluorescence-activated cell sorting (FACS) analysis demonstrated a significantly decreased frequency and number of ROR γ t $^{+}$ cells in the LNs and CNS of the SR12418-treated mice relative to vehicle controls (Figure 6D). The absolute number of GM-CSF $^{+}$ T cells was significantly lower in the SR12418 treated mice as was the frequency and number of IL-17A $^{+}$ and pathogenic IL-17A $^{+}$ IFN γ $^{+}$ cells in the LNs and CNS than mice receiving vehicle control (Figures 6C and 6E). Thus, targeted pharmacological modulation of REV-ERB activity *in vivo* effectively suppresses the development and progression of $\text{T}_{\text{H}}17$ -driven EAE.

To further evaluate the therapeutic efficacy of SR12418, we first performed intervention studies utilizing the adoptive T cell transfer model of colitis (Kjelle et al., 2006; Lindebo Holm et al., 2012) (Figure 7A). Following procedures described above, at 3-weeks after T cell transfer, SR12418 (50 mg/kg, b.i.d.) or vehicle control was administered twice daily for the duration of the experiment. PBS was used as a control. Neither group displayed any overt difference in body weight, colon weight, colon length, or colon weight/length ratio over time (Figure S7B). However, FACS analysis of colon tissue revealed that SR12418 led to a reduction in the frequency of $\alpha 4\beta 7^{+}$ T cells relative to vehicle controls, suggesting SR12418 hampered the ability of the T cells to home to the intestines (Figure 7B). Intracellular FACS analysis demonstrated a decreased frequency of ROR γ t $^{+}$ cells in the colons of the SR12418-treated mice relative to vehicle controls, whereas the frequency of IL-17A $^{+}$ and pathogenic IL-17A $^{+}$ IFN γ $^{+}$ cells was also lower than mice receiving vehicle control (Figures 7C and 7D). Interestingly, the frequency of CD25 $^{+}$ Foxp3 $^{+}$ Tregs was significantly increased in the colons of SR12418-treated mice relative to the vehicle controls (Figure 7E).

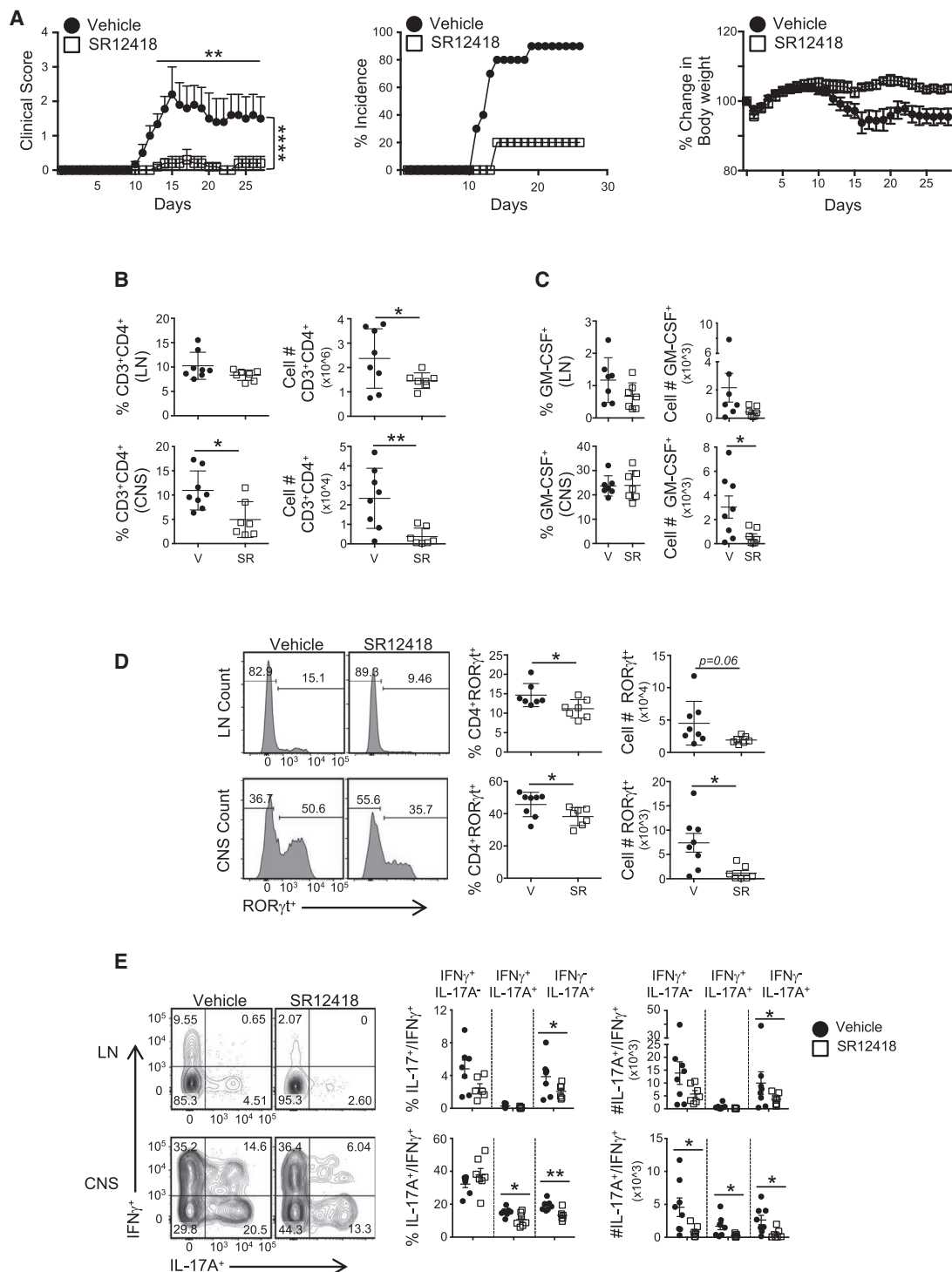
We next tested the therapeutic capacity of SR12418 for treating ongoing PLP_{139–151}-induced relapsing-remitting EAE (R-EAE) in SJL/J mice. SR12418 (50 mg/kg, b.i.d.) or vehicle control was

(D) Quantitative real-time PCR of $\text{T}_{\text{H}}17$ -mediated cytokines in cells treated with vehicle (DMSO), SR9009 (5 μ M), or SR12418 (5 μ M). Analysis was performed at 96 hr after T cell activation and compared to naive CD4 $^{+}$ T cells. β -actin was used as the internal control. Data represent mean \pm SEM ($n = 3$).

(E) FACS analysis of IL-17A and IFN γ expression in $\text{T}_{\text{H}}17$ cells transduced with MIGR1 ROR γ t and treated with vehicle (DMSO), SR9009, or SR12418 for 48 hr at the indicated doses. Cells were gated on live, GFP $^{+}$ cells ($n = 4$).

(F) FACS analysis of thymocytes from mice treated with vehicle, SR2211, SR9009, or SR12418 for 72 hr.

Graphs depict quantification of total thymocyte number, double positive percentage, and double positive number in each group ($n = 5$ /group). Data represent mean \pm SEM. * $p < 0.05$, ** $p < 0.01$, *** $p < 0.001$, **** $p < 0.0001$ determined using Student's t test. ns, not significant ($p > 0.05$).

**Figure 6. SR12418 Potently Suppresses the Development and Severity of EAE**

(A) Clinical EAE scores (left) from mice subjected to MOG-induced EAE and treated with vehicle (10/10/80 formulation of DMSO/Tween80/H₂O) or SR12418 (i.p., 50mg/kg, b.i.d.) for the duration of the experiment. Middle and right graphs demonstrate the percent incidence of disease and percent change in body weight over time between groups, respectively (n = 8–10/group).

(B) Frequencies and cell counts of CD3⁺CD4⁺ cells in the draining LNs and CNS of mice at peak of disease. V, vehicle; SR, SR12418-treated mice (n = 8; V; n = 7, SR).

(C) Graphs depicting the frequencies and cell counts of CD4⁺GM-CSF⁺ cells in LN and CNS of mice at peak of disease.

(legend continued on next page)

administered twice daily once mice had recovered from the first wave of disease (day 18 post-immunization). SR12418 resulted in a significant reduction in the relapse severity compared to the animals receiving vehicle control (Figure 7F). Twelve of the 17 mice in the vehicle-treated group relapsed, with the average maximum relapsing clinical score for each mouse recorded between 2.5 and 3.5. In contrast, only 5 of the 17 SR12418-treated animals relapsed, with the maximum clinical score recorded as no greater than 1. FACS analysis of the CNS from the animals revealed a significant decrease in the frequency and number of CD4⁺ and CD8⁺ effector cells (CD44^{hi}) in the SR12418-treated animals versus vehicle control (Figure 7G), which may be attributed to a decreased frequency and number of CD4⁺CCR6⁺ T cells in the CNS (Figure 7H). Intracellular FACS analysis demonstrated a decreased frequency and number of ROR γ t⁺ cells in the CNS of the SR12418-treated mice relative to vehicle controls, whereas the number of ROR γ t⁺GM-CSF⁺ cells was also decreased (Figures 7I and 7J). Finally, SR12418-treated animals demonstrated a decreased frequency of IL-17A⁺ cells and decreased number of IL-17A⁺ and pathogenic IL-17A⁺IFN γ ⁺ cells in CNS compared to mice receiving the vehicle control (Figure 7K). These results offer proof-of-concept that pharmacological modulation of REV-ERB activity post-disease onset can suppress the progression of T_H17-driven autoimmunity and chronic inflammatory disorders.

DISCUSSION

In this study, we demonstrated that REV-ERB α is induced exclusively in T_H17 cells and acts as a cell-intrinsic negative regulator of pro-inflammatory T_H17-cell function. Our results suggest that the induction of REV-ERB α represents a previously undefined and critical checkpoint during T_H17 cell development. Overexpression of REV-ERB α inhibited T_H17 cell development whereas its deletion led to increased pro-inflammatory cytokine production *in vitro* and *in vivo*, which is consistent with its role as a repressor of gene transcription (Kojetin and Burris, 2014). Mechanistically, REV-ERB α competes with ROR γ t for binding to the same RORE and/or RevRE genomic response sequence at the *Il17a* locus, which was further supported by the overlap in gene signatures between WT/KO and WT/ROR γ t^{-/-} T_H17 cells. REV-ERB α bound upstream of the *Rorc* transcriptional start site, suggesting it also regulated T_H17 cell development through repression of ROR γ t itself. Finally, REV-ERB-specific small molecules suppressed T_H17 cell development *in vitro* and were extremely effective when used prophylactically in suppressing T_H17-mediated autoimmunity *in vivo*. Importantly, SR12418 was effective when used in a therapeutic mode in two separate models of T_H17-mediated inflammatory diseases, colitis, and EAE. Collectively, these findings demonstrate that the nuclear receptor REV-ERB α is a cell-intrinsic negative regulator of T_H17 cell development whose activity is critical for dampening pro-inflammatory cytokine production.

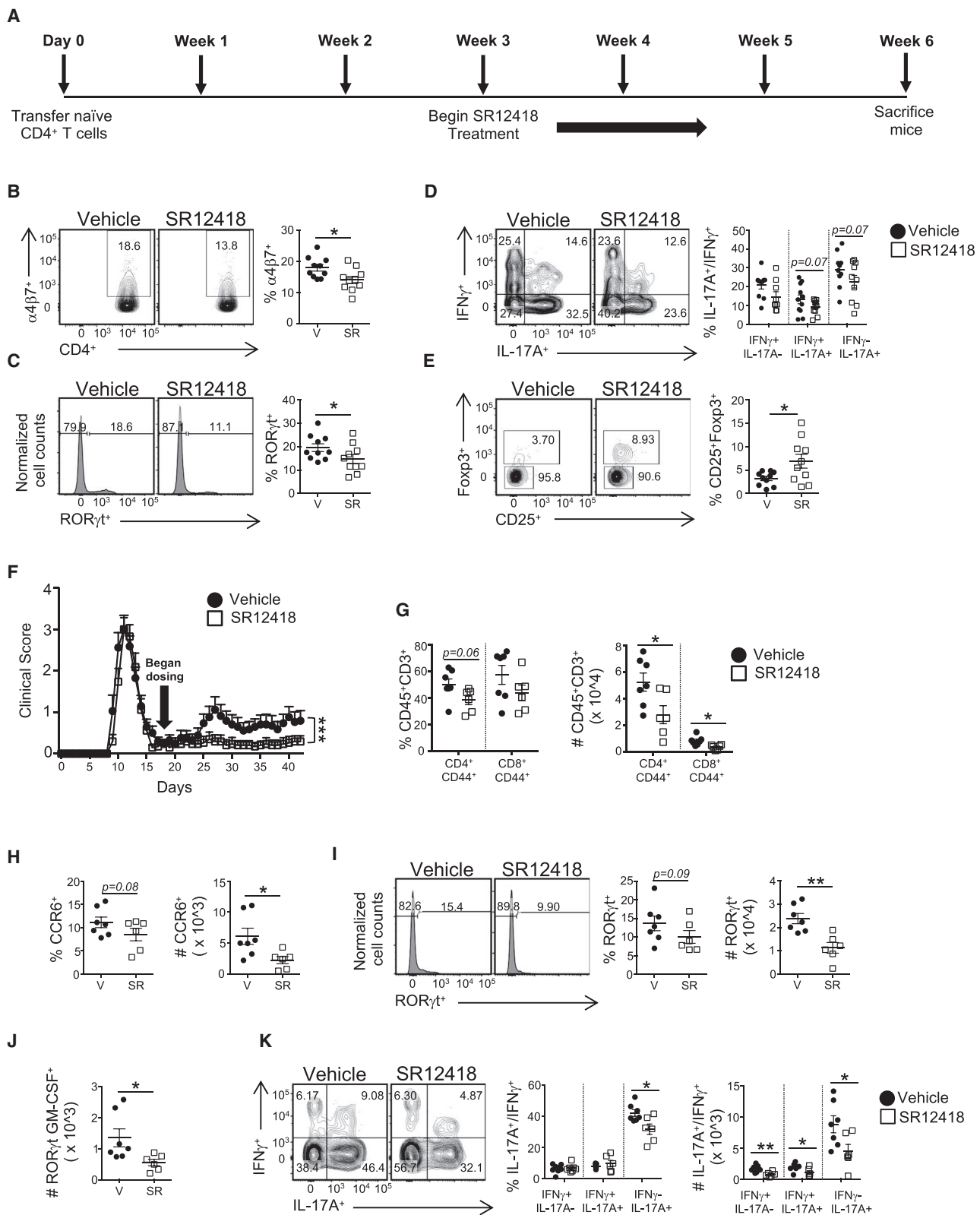
Although cross-talk between the RORs and REV-ERBs is well established in the regulation of the circadian rhythm and metabolic processes, cross-talk between these receptors has not been extensively explored in the immune system. Here, we demonstrate that REV-ERB α competes with ROR γ t at their shared RORE and/or RevRE sites, including the *Il17a* locus to regulate IL-17A cytokine expression. Comparison of the KO and ROR γ t^{-/-} T_H17 cell RNA sequencing (RNA-seq) datasets suggests there is overlap in the genes that have clear RORE and/or RevREs in their promoter regions, including *Il17f*, *Ccl20*, and *Ltb4r1*. Although many genes did not overlap with the ROR γ t^{-/-} T_H17 cells, many of these were downregulated in KO T_H17 cells, likely indicating that REV-ERB α was indirectly regulating those genes. Of the other non-ROR γ overlapping genes that were upregulated in KO T_H17 cells, these repressive effects could be a function of DNA-independent mechanisms, otherwise known as tethering, in which REV-ERB α binds to cell-type-specific transcription factors to negatively regulate gene transcription to convey a tissue-specific genetic program tailored to the needs of that cell type (Zhang et al., 2015). In metabolic tissues such as the liver, these two different modes of repression enable REV-ERB α the ability to stabilize the circadian oscillations of clock genes at RORE and/or RevREs while coupling metabolism to environmental and metabolic changes (Zhang et al., 2015). Perhaps a comparable phenomenon endows REV-ERB α the ability to function in a similar manner in T_H17 cells. More in-depth ChIP and ChIP sequencing studies will need to be performed to establish these different modes of REV-ERB-mediated repression.

REV-ERB α also appears to regulate the expression of ROR γ t, and although consistent with previously published work (Cho et al., 2012; Mongrain et al., 2008), we do not believe the majority of effects observed *in vitro* and *in vivo* on T_H17 cell function, including IL-17A expression, are due to REV-ERB α -dependent effects on ROR γ t expression. Mechanistically, binding of REV-ERB α upstream of *Rorc* would negatively regulate ROR γ t expression and, in turn, indirectly regulate IL-17A expression *in vitro* and *in vivo*. Therefore, the loss of REV-ERB α would have the opposite effect, and one could argue that this would be the sole mechanism for REV-ERB α -mediated regulation of T_H17 cell development. However, decreased IL-17A expression was also observed when ROR γ t was ectopically overexpressed in T_H17 cells and REV-ERB-specific small molecules were added to the culture. Since the expression of ROR γ t is driven by a retroviral element, REV-ERB α could not regulate ROR γ t at this level. Thus, our data indicate a level of complexity to the cross-talk between the RORs and REV-ERBs in T_H17 cell development that extends beyond simple competition for DNA response elements. At one level, ROR γ t and REV-ERB α compete for binding at the *Il17a* locus to contain the inflammatory response. At another level, the RORs and REV-ERB α drive and inhibit each other's expression (Raspè et al., 2002; Takeda et al., 2012), with the RORs potentially driving REV-ERB α .

(D) FACS analysis, frequencies, and cell counts of ROR γ t⁺ cells in LNs and CNS of mice at peak of disease.

(E) FACS analysis, frequencies, and cell counts of IL-17A⁺IFN γ ⁻, IL-17A⁺IFN γ ⁺, and IL-17A⁺IFN γ ⁺ cells in the LN and CNS of mice at peak of disease.

Cells were gated on live, CD45⁺CD3⁺CD4⁺ cells. Data are mean \pm SEM and representative of three separate, independent experiments with similar results. Two-way ANOVA (clinical score) and Student's t tests were performed for statistical analysis. *p < 0.05, **p < 0.01, ***p < 0.001, ****p < 0.0001.



(legend on next page)

expression upon development in order for REV-ERB α to limit not only cytokine expression but also expression of ROR γ t itself to help temper T H 17 pro-inflammatory responses.

Our observations that REV-ERB α acts as a potent negative regulator of pro-inflammatory T H 17 cell development and autoimmunity contradicts a previous study by Yu et al. (2013) where they demonstrated that REV-ERB α functionally repressed Nfil3, which, in turn, repressed ROR γ t to regulate *Il17a* expression and T H 17 cell development, indicating an indirect role for REV-ERB α in the regulation of T H 17 cell development. In the study by Yu et al. (2013), KO mice presented with decreased IL-17A expression *in vitro* and *in vivo*, and although the different gut flora compositions between the facilities could be a factor affecting the development of T H 17 cells (Lee and Kim, 2017; Luo et al., 2017; Yang et al., 2014), or the use of different REV-ERB α KO strains (Chomez et al., 2000; Preitner et al., 2002), it is important to note that the studies performed by Yu et al. (2013) were largely in naive mice with the purpose of elucidating the diurnal regulation of T H 17 cell function *in vivo*. In that setting, REV-ERB α and NFIL3 cooperatively regulated T H 17 cells in the gut in a clock-dependent manner (Yu et al., 2013). In contrast, our work was performed under specific autoimmune- or chronic pro-inflammatory-inducing conditions, which are known to be T H 17 driven, to specifically address the role of REV-ERB α outside of its function as a core clock component. Under the types of stressors used in our study here, REV-ERB α is required to restrain pro-inflammatory responses, and in the absence of REV-ERB α , aberrant T H 17 responses and autoimmunity ensue. Supporting this notion, microarray analysis of CNS tissues (Pareek et al., 2011), RNA-sequencing of spinal cords (Sevastou et al., 2016), and mRNA analysis of CNS (Sutton et al., 2017) from mice with active EAE all demonstrate a significant decrease in REV-ERB α expression. These data correlate with the findings from our EAE experiments, wherein the loss of REV-ERB α exacerbates EAE, and enhanced REV-ERB activity, through use small molecules agonists (SR9009 or SR12418), suppresses EAE. Additionally, we showed that T cell-specific loss of REV-ERB α exacerbated the development of colitis, further supporting the notion that REV-ERB α acts as a critical negative regulator of pro-inflammatory T H 17-mediated responses.

Despite the *in vivo* differences between our study and Yu et al. (2013), we did observe REV-ERB-mediated effects on Nfil3 in T H 17 cells, which was likely a function of REV-ERB α binding at the Nfil3 promoter region. However, the effects do not appear to be sufficient to override the direct effects of REV-ERB α at *Il17a* or ROR γ t itself, as we observed reduced IL-17A expression in REV-ERB α -overexpressing cells and cells treated with a syn-

thetic REV-ERB ligand. Interestingly, despite the increased expression of Nfil3 in KO T H 17 cells, we still observed an increased expression of ROR γ t and IL-17A (Yu et al., 2013). This could be a function of protein degradation because NFIL3 has been shown to be post-translationally modified and targeted for proteasomal degradation in a CK1 ϵ -dependent manner (Doi et al., 2004). However, overexpression and knock down of Nfil3 also had little effect on IL-17A expression, which is consistent with a previous study (Ciofani et al., 2012) finding that retroviral transduction of Nfil3 did not significantly affect T H 17 cell development. This conflicting *in vitro* data could be due to differences in cell culture conditions, reagents, or transduction protocols. Clearly the network linking REV-ERB α and NFIL3 in T H 17 cells is complex and further work is needed to elucidate the interplay between these transcription factors in pro-inflammatory T H 17 cell development. Overall, our data provide a new perspective on REV-ERB α , revealing its negative regulatory role of pro-inflammatory T H 17-mediated immune responses.

Modulation of nuclear receptor activity has proven to be a powerful and effective means to treat a host of diseases (Mariano et al., 2014). We have developed and described several REV-ERB-specific small molecules exhibiting various degrees of *in vivo* exposure (Solt et al., 2012). Using these small molecules, we demonstrated that REV-ERB agonism is sufficient to inhibit T H 17 cell development *in vitro* by inhibiting T H 17-specific genes (e.g., *Il17a*, *Il22*, and *Il23r*) as well as ROR γ t expression, which is consistent with our genetic experiments. Furthermore, REV-ERB-specific small molecules also inhibit the development of T H 17 cells *in vivo*, ameliorating the signs and incidence of EAE, a T H 17-mediated autoimmune disease. Importantly, REV-ERB-specific small molecules are efficacious when used therapeutically, blocking the development of colitis and preventing disease relapse in a relapsing-remitting model of multiple sclerosis. It is possible that some of the *in vivo* effects observed with SR12418 are a function of systemic exposure, which would target the REV-ERBs in other tissues, including macrophages, which have been demonstrated to express the REV-ERBs and can act as antigen-presenting cells (Eichenfield et al., 2016; Gibbs et al., 2012; Lam et al., 2013). Additionally, SR12418 and SR9009 target both REV-ERB α and REV-ERB β , and although the focus of this work was on REV-ERB α , our data do not rule out effects on REV-ERB β . In fact, REV-ERB β is differentially expressed in T H 17 cells, and its overexpression did inhibit T H 17-mediated cytokine expression, but it was not as potent as REV-ERB α . Thus, the combined deletion of both REV-ERBs may have a more exacerbated effect *in vivo* on disease course.

Figure 7. SR12418 Is Effective When Used in Intervention Studies of Colitis and Relapsing-Remitting EAE

(A) Schematic of the adoptive T cell transfer colitis model treatment design.
 (B-E) FACS plots and graphs demonstrating frequencies of (B) α 4 β 7 $^+$, (C) ROR γ t $^+$, (D) IL-17A $^+$ IFN γ $^-$, IL-17A $^+$ IFN γ $^+$, and IL-17A $^+$ IFN γ $^+$, and (E) CD25 $^+$ Foxp3 $^+$ T cells in the colons of recipient mice. Cells were gated on live, CD45 $^+$ CD3 $^+$ CD4 $^+$ cells. V, vehicle; SR, SR12418. Data are mean \pm SEM (n = 10/group; PBS, n = 2).
 (F) Clinical EAE scores from mice subjected to PLP-induced EAE and treated with vehicle or SR12418 (i.p., 50 mg/kg, b.i.d.) starting on day 18 and continued for the duration of the experiment (n = 17/group).
 (G-K) Graphs demonstrating decreased frequencies and cell numbers of (G) effector CD4 and CD8 T cells and (H) CCR6 $^+$ T cells in the CNS of mice treated with SR12418. FACS plots and graphs demonstrating frequencies and/or cell numbers of (I) ROR γ t $^+$, (J) ROR γ t $^+$ GM-CSF $^+$, and (K) IL-17A $^+$ IFN γ $^-$, IL-17A $^+$ IFN γ $^+$, and IL-17A $^+$ IFN γ $^+$ T cells in the CNS of SR12418-treated mice relative to vehicle controls.
 Cells were gated on live, CD45 $^+$ CD3 $^+$ CD4 $^+$ CD44 $^+$ cells (n = 7, vehicle; n = 6, SR12418). Data represent mean \pm SEM. Two-way ANOVA (clinical score) and Student's t tests were performed for statistical analysis. *p < 0.05, **p < 0.01, ***p < 0.001.

By this logic, it would stand to reason that ligands that target both REV-ERBs would also have a greater repressive effect than a ligand that targeted only a single receptor subtype.

In summary, we demonstrate here that the nuclear receptor REV-ERB α is a critical, cell-intrinsic negative regulator of pro-inflammatory T H 17-mediated autoimmunity, competing with ROR γ t at their shared target gene sequences, of which *Il17a* is one. Although there is still much work to be done to fully elucidate the function of REV-ERB α in T H 17 cells, our work also demonstrates the therapeutic potential for targeting REV-ERB α for the treatment of T H 17-mediated autoimmune disorders. Currently, there is a massive pharmaceutical effort to develop ROR γ -selective inverse agonists for the treatment of T H 17-mediated disorders. However, these ROR γ synthetic ligands phenocopy *Rorc*^{-/-} mice by rapidly inducing thymic apoptosis, whereas REV-ERB ligands do not. Our data indicate that the use of REV-ERB-specific small molecules may be an effective, alternative approach to treat T H 17-mediated diseases.

STAR METHODS

Detailed methods are provided in the online version of this paper and include the following:

- KEY RESOURCES TABLE
- CONTACT FOR REAGENT AND RESOURCE SHARING
- EXPERIMENTAL MODEL AND SUBJECT DETAILS
 - Animals
 - Cell lines
- METHOD DETAILS
 - Chemical synthesis and reagents
 - Induction and clinical evaluation of EAE
 - T cell-transfer colitis model
 - Analysis of thymocytes
 - *In vitro* CD4 $^+$ T cell differentiation
 - Flow cytometry
 - Retroviral Transduction
 - Luciferase reporter assays
 - ChIP
 - Quantitative real-time PCR
 - RNA-sequencing and data analysis
 - TR-FRET corepressor interaction assay
 - Immunoblot Analysis
- QUANTIFICATION AND STATISTICAL ANALYSIS
- DATA AND SOFTWARE AVAILABILITY

SUPPLEMENTAL INFORMATION

Supplemental Information includes seven figures and three tables and can be found with this article online at <https://doi.org/10.1016/j.celrep.2018.11.101>.

ACKNOWLEDGMENTS

We thank the members of the Pipkin and Sundrud labs for their helpful comments and critiques of experimental design and analysis as well as the Scripps Florida Genomics and Scripps Florida and California Bioinformatics Cores for library preparation, RNA-seq, and data analysis. This work was supported by the Margaret Q. Landenberger Foundation and the NIH (1R01AI116885 to L.A.S.; 1R01GM114420 to D.J.K.). L.B.C. was supported by NSF award 1359369. M.A. was supported through the American Association of Immunol-

ogists Careers in Immunology Fellowship Program and the Crohn's and Colitis Foundation of America (546172).

AUTHOR CONTRIBUTIONS

L.A.S. conceived the project; Y.H., C.D., and T.M.K. synthesized and analyzed the ligands; L.A.S., S.C., M.A., S.C., S.A.M., and L.B.C. designed/analyzed, and/or performed the *in vitro* assays; J.S. and D.J.K. designed/analyzed and/or performed TR-FRET assays; L.A.S., S.C., M.A., R.W., O.B.P., and S.C. designed, analyzed, and/or performed the *in vivo* studies; M.D.C. performed the pharmacokinetic analysis; L.A.S. wrote the manuscript with input from all of the authors.

DECLARATION OF INTERESTS

The authors declare no competing financial interests.

Received: February 16, 2018

Revised: September 19, 2018

Accepted: November 29, 2018

Published: December 26, 2018

REFERENCES

- Anders, S., and Huber, W. (2010). Differential expression analysis for sequence count data. *Genome Biol.* 11, R106.
- Banerjee, S., Wang, Y., Solt, L.A., Griffett, K., Kazantzis, M., Amador, A., El-Gendy, B.M., Huitron-Resendiz, S., Roberts, A.J., Shin, Y., et al. (2014). Pharmacological targeting of the mammalian clock regulates sleep architecture and emotional behaviour. *Nat. Commun.* 5, 5759.
- Bronner, S.M., Zbieg, J.R., and Crawford, J.J. (2017). ROR γ antagonists and inverse agonists: a patent review. *Expert Opin. Ther. Pat.* 27, 101–112.
- Chang, M.R., Lyda, B., Kamenecka, T.M., and Griffin, P.R. (2014). Pharmacologic repression of retinoic acid receptor-related orphan nuclear receptor γ is therapeutic in the collagen-induced arthritis experimental model. *Arthritis Rheumatol.* 66, 579–588.
- Chen, R., Belanger, S., Frederick, M.A., Li, B., Johnston, R.J., Xiao, N., Liu, Y.C., Sharma, S., Peters, B., Rao, A., et al. (2014). *In vivo* RNA interference screens identify regulators of antiviral CD4(+) and CD8(+) T cell differentiation. *Immunity* 41, 324–338.
- Cho, J.H. (2008). The genetics and immunopathogenesis of inflammatory bowel disease. *Nat. Rev. Immunol.* 8, 458–466.
- Cho, H., Zhao, X., Hatori, M., Yu, R.T., Barish, G.D., Lam, M.T., Chong, L.W., DiTacchio, L., Atkins, A.R., Glass, C.K., et al. (2012). Regulation of circadian behaviour and metabolism by REV-ERB- α and REV-ERB- β . *Nature* 485, 123–127.
- Chomez, P., Neveu, I., Mansén, A., Kiesler, E., Larsson, L., Vennström, B., and Arenas, E. (2000). Increased cell death and delayed development in the cerebellum of mice lacking the rev-erbA(alpha) orphan receptor. *Development* 127, 1489–1498.
- Ciofani, M., Madar, A., Galan, C., Sellars, M., Mace, K., Pauli, F., Agarwal, A., Huang, W., Parkhurst, C.N., Muratet, M., et al. (2012). A validated regulatory network for Th17 cell specification. *Cell* 151, 289–303.
- Doi, M., Okano, T., Yujnovsky, I., Sassone-Corsi, P., and Fukada, Y. (2004). Negative control of circadian clock regulator E4BP4 by casein kinase I epsilon-mediated phosphorylation. *Curr. Biol.* 14, 975–980.
- Eichenfield, D.Z., Troutman, T.D., Link, V.M., Lam, M.T., Cho, H., Gosselin, D., Spann, N.J., Lesch, H.P., Tao, J., Muto, J., et al. (2016). Tissue damage drives co-localization of NF- κ B, Smad3, and Nrf2 to direct Rev-erb sensitive wound repair in mouse macrophages. *eLife* 5, e13024.
- Everett, L.J., and Lazar, M.A. (2014). Nuclear receptor Rev-erb α : up, down, and all around. *Trends Endocrinol. Metab.* 25, 586–592.

- Fellmann, C., Hoffmann, T., Sridhar, V., Hopfgartner, B., Muhar, M., Roth, M., Lai, D.Y., Barbosa, I.A., Kwon, J.S., Guan, Y., et al. (2013). An optimized microRNA backbone for effective single-copy RNAi. *Cell Rep.* 5, 1704–1713.
- Ghoreschi, K., Laurence, A., Yang, X.P., Tato, C.M., McGeachy, M.J., Konkel, J.E., Ramos, H.L., Wei, L., Davidson, T.S., Bouladoux, N., et al. (2010). Generation of pathogenic T(H)17 cells in the absence of TGF- β signalling. *Nature* 467, 967–971.
- Gibbs, J.E., Blaikley, J., Beesley, S., Matthews, L., Simpson, K.D., Boyce, S.H., Farrow, S.N., Else, K.J., Singh, D., Ray, D.W., and Loudon, A.S. (2012). The nuclear receptor REV-ERB α mediates circadian regulation of innate immunity through selective regulation of inflammatory cytokines. *Proc. Natl. Acad. Sci. USA* 109, 582–587.
- Guo, Y., MacIsaac, K.D., Chen, Y., Miller, R.J., Jain, R., Joyce-Shaikh, B., Ferguson, H., Wang, I.M., Cristescu, R., Mudgett, J., et al. (2016). Inhibition of ROR γ T skews TCR α gene rearrangement and limits t cell repertoire diversity. *Cell Rep.* 17, 3206–3218.
- Harbour, S.N., Maynard, C.L., Zindl, C.L., Schoeb, T.R., and Weaver, C.T. (2015). Th17 cells give rise to Th1 cells that are required for the pathogenesis of colitis. *Proc. Natl. Acad. Sci. USA* 112, 7061–7066.
- Hirota, K., Duarte, J.H., Veldhoen, M., Hornsby, E., Li, Y., Cua, D.J., Ahlfors, H., Wilhelm, C., Tolaini, M., Menzel, U., et al. (2011). Fate mapping of IL-17-producing T cells in inflammatory responses. *Nat. Immunol.* 12, 255–263.
- Huang, W., Sherman, B.T., and Lempicki, R.A. (2009a). Bioinformatics enrichment tools: paths toward the comprehensive functional analysis of large gene lists. *Nucleic Acids Res.* 37, 1–13.
- Huang, W., Sherman, B.T., and Lempicki, R.A. (2009b). Systematic and integrative analysis of large gene lists using DAVID bioinformatics resources. *Nat. Protoc.* 4, 44–57.
- Huh, J.R., Leung, M.W., Huang, P., Ryan, D.A., Krout, M.R., Malapaka, R.R., Chow, J., Manel, N., Ciofani, M., Kim, S.V., et al. (2011). Digoxin and its derivatives suppress Th17 cell differentiation by antagonizing ROR γ T activity. *Nature* 472, 486–490.
- Ivanov, I.I., McKenzie, B.S., Zhou, L., Tadokoro, C.E., Lepelley, A., Lafaille, J.J., Cua, D.J., and Littman, D.R. (2006). The orphan nuclear receptor ROR γ mat directs the differentiation program of proinflammatory IL-17+ T helper cells. *Cell* 126, 1121–1133.
- Jostins, L., Ripke, S., Weersma, R.K., Duerr, R.H., McGovern, D.P., Hui, K.Y., Lee, J.C., Schumm, L.P., Sharma, Y., Anderson, C.A., et al.; International IBD Genetics Consortium (IIBDGC) (2012). Host-microbe interactions have shaped the genetic architecture of inflammatory bowel disease. *Nature* 491, 119–124.
- Kjellev, S., Lundsgaard, D., Poulsen, S.S., and Markholst, H. (2006). Reconstitution of Scid mice with CD4+CD25- T cells leads to rapid colitis: an improved model for pharmacologic testing. *Int. Immunopharmacol.* 6, 1341–1354.
- Kojetin, D.J., and Burris, T.P. (2014). REV-ERB and ROR nuclear receptors as drug targets. *Nat. Rev. Drug Discov.* 13, 197–216.
- Kojetin, D., Wang, Y., Kamenecka, T.M., and Burris, T.P. (2011). Identification of SR8278, a synthetic antagonist of the nuclear heme receptor REV-ERB. *ACS Chem. Biol.* 6, 131–134.
- Kumar, N., Lyda, B., Chang, M.R., Lauer, J.L., Solt, L.A., Burris, T.P., Kamenecka, T.M., and Griffin, P.R. (2012). Identification of SR2211: a potent synthetic ROR γ -selective modulator. *ACS Chem. Biol.* 7, 672–677.
- Kurebayashi, S., Ueda, E., Sakae, M., Patel, D.D., Medvedev, A., Zhang, F., and Jetten, A.M. (2000). Retinoid-related orphan receptor gamma (ROR γ) is essential for lymphoid organogenesis and controls apoptosis during thymopoiesis. *Proc. Natl. Acad. Sci. USA* 97, 10132–10137.
- Lam, M.T., Cho, H., Lesch, H.P., Gosselin, D., Heinz, S., Tanaka-Oishi, Y., Benner, C., Kaikkonen, M.U., Kim, A.S., Kosaka, M., et al. (2013). Rev-Erb α represses macrophage gene expression by inhibiting enhancer-directed transcription. *Nature* 498, 511–515.
- Lee, N., and Kim, W.U. (2017). Microbiota in T-cell homeostasis and inflammatory diseases. *Exp. Mol. Med.* 49, e340.
- Lee, Y.K., Turner, H., Maynard, C.L., Oliver, J.R., Chen, D., Elson, C.O., and Weaver, C.T. (2009). Late developmental plasticity in the T helper 17 lineage. *Immunity* 30, 92–107.
- Lee, Y., Awasthi, A., Yosef, N., Quintana, F.J., Xiao, S., Peters, A., Wu, C., Kleinewietfeld, M., Kunder, S., Hafler, D.A., et al. (2012). Induction and molecular signature of pathogenic Th17 cells. *Nat. Immunol.* 13, 991–999.
- Lees, C.W., Barrett, J.C., Parkes, M., and Satsangi, J. (2011). New IBD genetics: common pathways with other diseases. *Gut* 60, 1739–1753.
- Lindebo Holm, T., Poulsen, S.S., Markholst, H., and Reedtz-Runge, S. (2012). Pharmacological evaluation of the SCID T cell transfer model of colitis: as a model of Crohn's disease. *Int. J. Inflamm.* 2012, 412178.
- Luo, A., Leach, S.T., Barres, R., Hesson, L.B., Grimm, M.C., and Simar, D. (2017). The microbiota and epigenetic regulation of T helper 17/regulatory T cells: in search of a balanced immune system. *Front. Immunol.* 8, 417.
- Marciano, D.P., Chang, M.R., Corzo, C.A., Goswami, D., Lam, V.Q., Pascal, B.D., and Griffin, P.R. (2014). The therapeutic potential of nuclear receptor modulators for treatment of metabolic disorders: PPAR γ , RORs, and Rev-erbs. *Cell Metab.* 19, 193–208.
- Matta-Camacho, E., Banerjee, S., Hughes, T.S., Solt, L.A., Wang, Y., Burris, T.P., and Kojetin, D.J. (2014). Structure of REV-ERB β ligand-binding domain bound to a porphyrin antagonist. *J. Biol. Chem.* 289, 20054–20066.
- McGeachy, M.J., and Cua, D.J. (2008). Th17 cell differentiation: the long and winding road. *Immunity* 28, 445–453.
- Mombaerts, P., Iacomini, J., Johnson, R.S., Herrup, K., Tonegawa, S., and Papaioannou, V.E. (1992). RAG-1-deficient mice have no mature B and T lymphocytes. *Cell* 68, 869–877.
- Mongrain, V., Ruan, X., Dardente, H., Fortier, E.E., and Cermakian, N. (2008). Clock-dependent and independent transcriptional control of the two isoforms from the mouse Rorgamma gene. *Genes Cells* 13, 1197–1210.
- Nair, R.P., Duffin, K.C., Helms, C., Ding, J., Stuart, P.E., Goldgar, D., Gudjonsson, J.E., Li, Y., Tejasvi, T., Feng, B.J., et al.; Collaborative Association Study of Psoriasis (2009). Genome-wide scan reveals association of psoriasis with IL-23 and NF-kappaB pathways. *Nat. Genet.* 41, 199–204.
- Naviaux, R.K., Costanzi, E., Hass, M., and Verma, I.M. (1996). ThepCL vector system: rapid production of helper-free, high-titer, recombinant retrovirus. *J. Virol.* 70, 5701–5705.
- Noel, R., Song, X., Shin, Y., Banerjee, S., Kojetin, D., Lin, L., Ruiz, C.H., Cameron, M.D., Burris, T.P., and Kamenecka, T.M. (2012). Synthesis and SAR of tetrahydroisoquinolines as Rev-erb α agonists. *Bioorg. Med. Chem. Lett.* 22, 3739–3742.
- Pareek, T.K., Belkadi, A., Kesavapany, S., Zaremba, A., Loh, S.L., Bai, L., Cohen, M.L., Meyer, C., Liby, K.T., Miller, R.H., et al. (2011). Triterpenoid modulation of IL-17 and Nrf-2 expression ameliorates neuroinflammation and promotes remyelination in autoimmune encephalomyelitis. *Sci. Rep.* 1, 201.
- Peters, A., Lee, Y., and Kuchroo, V.K. (2011). The many faces of Th17 cells. *Curr. Opin. Immunol.* 23, 702–706.
- Preitner, N., Damiola, F., Lopez-Molina, L., Zakany, J., Duboule, D., Albrecht, U., and Schibler, U. (2002). The orphan nuclear receptor REV-ERB α controls circadian transcription within the positive limb of the mammalian circadian oscillator. *Cell* 110, 251–260.
- Raghuram, S., Stayrook, K.R., Huang, P., Rogers, P.M., Nosie, A.K., McClure, D.B., Burris, L.L., Khorasanizadeh, S., Burris, T.P., and Rastinejad, F. (2007). Identification of heme as the ligand for the orphan nuclear receptors REV-ERB α and REV-ERB β . *Nat. Struct. Mol. Biol.* 14, 1207–1213.
- Raspè, E., Mautino, G., Duval, C., Fontaine, C., Duez, H., Barbier, O., Monte, D., Fruchart, J., Fruchart, J.C., and Staels, B. (2002). Transcriptional regulation of human Rev-erbalpha gene expression by the orphan nuclear receptor retinoic acid-related orphan receptor alpha. *J. Biol. Chem.* 277, 49275–49281.
- Sebastou, I., Pryce, G., Baker, D., and Selwood, D.L. (2016). Characterisation of transcriptional changes in the spinal cord of the progressive experimental autoimmune encephalomyelitis Biozzi ABH mouse model by RNA sequencing. *PLoS One* 11, e0157754.

- Solt, L.A., Kumar, N., Nuhant, P., Wang, Y., Lauer, J.L., Liu, J., Istrate, M.A., Kamenecka, T.M., Roush, W.R., Vidović, D., et al. (2011). Suppression of Th17 differentiation and autoimmunity by a synthetic ROR ligand. *Nature* **472**, 491–494.
- Solt, L.A., Wang, Y., Banerjee, S., Hughes, T., Kojetin, D.J., Lundasen, T., Shin, Y., Liu, J., Cameron, M.D., Noel, R., et al. (2012). Regulation of circadian behaviour and metabolism by synthetic REV-ERB agonists. *Nature* **485**, 62–68.
- Sun, Z., Unutmaz, D., Zou, Y.R., Sunshine, M.J., Pierani, A., Brenner-Morton, S., Mebius, R.E., and Littman, D.R. (2000). Requirement for ROR γ in thymocyte survival and lymphoid organ development. *Science* **288**, 2369–2373.
- Sutton, C.E., Finlay, C.M., Raverdeau, M., Early, J.O., DeCourcey, J., Zaslona, Z., O'Neill, L.A.J., Mills, K.H.G., and Curtis, A.M. (2017). Loss of the molecular clock in myeloid cells exacerbates T cell-mediated CNS autoimmune disease. *Nat. Commun.* **8**, 1923.
- Takeda, Y., Jothi, R., Birault, V., and Jetten, A.M. (2012). ROR γ directly regulates the circadian expression of clock genes and downstream targets in vivo. *Nucleic Acids Res.* **40**, 8519–8535.
- Trapnell, C., Pachter, L., and Salzberg, S.L. (2009). TopHat: discovering splice junctions with RNA-Seq. *Bioinformatics* **25**, 1105–1111.
- Wang, R., Hasnain, S.Z., Tong, H., Das, I., Che-Hao Chen, A., Oancea, I., Proctor, M., Florin, T.H., Eri, R.D., and McGuckin, M.A. (2015). Neutralizing IL-23 is superior to blocking IL-17 in suppressing intestinal inflammation in a spontaneous murine colitis model. *Inflamm. Bowel Dis.* **21**, 973–984.
- Yang, X.O., Pappu, B.P., Nurieva, R., Akimzhanov, A., Kang, H.S., Chung, Y., Ma, L., Shah, B., Panopoulos, A.D., Schluns, K.S., et al. (2008). T helper 17 lineage differentiation is programmed by orphan nuclear receptors ROR alpha and ROR gamma. *Immunity* **28**, 29–39.
- Yang, Y., Torchinsky, M.B., Gobert, M., Xiong, H., Xu, M., Linehan, J.L., Alonzo, F., Ng, C., Chen, A., Lin, X., et al. (2014). Focused specificity of intestinal Th17 cells towards commensal bacterial antigens. *Nature* **510**, 152–156.
- Yin, L., Wu, N., Curtin, J.C., Qatanani, M., Szwerdgold, N.R., Reid, R.A., Waitt, G.M., Parks, D.J., Pearce, K.H., Wisely, G.B., and Lazar, M.A. (2007). Rev-erbalpha, a heme sensor that coordinates metabolic and circadian pathways. *Science* **318**, 1786–1789.
- Yin, L., Wu, N., and Lazar, M.A. (2010). Nuclear receptor Rev-erbalpha: a heme receptor that coordinates circadian rhythm and metabolism. *Nucl. Recept. Signal.* **8**, e001.
- Yu, W., Nomura, M., and Ikeda, M. (2002). Interactivating feedback loops within the mammalian clock: BMAL1 is negatively autoregulated and upregulated by CRY1, CRY2, and PER2. *Biochem. Biophys. Res. Commun.* **290**, 933–941.
- Yu, X., Rollins, D., Ruhn, K.A., Stubblefield, J.J., Green, C.B., Kashiwada, M., Rothman, P.B., Takahashi, J.S., and Hooper, L.V. (2013). Th17 cell differentiation is regulated by the circadian clock. *Science* **342**, 727–730.
- Zhang, F., Meng, G., and Strober, W. (2008). Interactions among the transcription factors Runx1, RORgammat and Foxp3 regulate the differentiation of interleukin 17-producing T cells. *Nat. Immunol.* **9**, 1297–1306.
- Zhang, Y., Fang, B., Emmett, M.J., Damle, M., Sun, Z., Feng, D., Armour, S.M., Remsberg, J.R., Jager, J., Soccio, R.E., et al. (2015). Gene regulation. Discrete functions of nuclear receptor Rev-erb α couple metabolism to the clock. *Science* **348**, 1488–1492.

STAR★METHODS

KEY RESOURCES TABLE

REAGENT or RESOURCE	SOURCE	IDENTIFIER
Antibodies		
LanthaScreen Elite Tb-anti-His Antibody	Thermo Fisher	Cat # PV5863
Mouse ROR γ t (immunoblot)	eBioscience	Cat # MA5-16227; RRID: AB_2537745
Actin, clone C4	EMD Millipore	Cat # MAB1501
Rabbit polyclonal anti-REV-ERB α	This paper	N/A
Purified anti IL-4, clone 11B11	Biolegend	Cat# 504115; RRID: AB_2295885
Purified anti-IFN γ , clone XMG1.2	Biolegend	Cat# 505834; RRID: AB_11150776
Soluble anti-CD3, clone 2C11	eBioscience	Cat# 16-0031-86; RRID: AB_468849
Soluble anti-CD28, clone 37.51	eBioscience	Cat# 16-0281-86; RRID: AB_468923
Goat anti-Hamster IgG	MP Biomedicals	Cat # 856984
BUV395 Hamster anti-mouse CD3e, clone 145-2C11	BD Biosciences	Cat# 563565; RRID: AB_2738278
BV711 anti-mouse CD4, clone RM4-5	Biolegend	Cat# 100549; RRID: AB_11219396
FITC anti-mouse CD8a, clone 53-6.7	eBioscience	Cat# 11-0081-85; RRID: AB_464916
FITC anti-mouse CD19, clone eBio1D3	eBioscience	Cat# 11-0193-86; RRID: AB_657665
BV605 anti-mouse CD25, clone PC61	Biolegend	Cat# 102035; RRID: AB_11126977
PerCP-Cy5.5 anti-mouse/human CD44, clone IM7	Biolegend	Cat# 103031; RRID: AB_2076206
A700 anti-mouse CD45, clone 30-F11	Biolegend	Cat# 103128; RRID: AB_493715
BV421 Rat anti-mouse CD62L, clone MEL-14	BD Biosciences	Cat# 562910; RRID: AB_2737885
eFluor 660 anti-mouse CCR6, clone sirx6	eBioscience	Cat# 50-7196-80; RRID: AB_11218711
Pe/Cy7 anti-mouse CXCR3, clone CXCR3-173	Biolegend	Cat# 126515; RRID: AB_2086740
FITC anti-mouse B220, clone RA3-6B2	eBioscience	Cat# 11-0452-82; RRID: AB_465054
eFluor 660 anti-mouse Foxp3, clone FJK-16 s	eBioscience	Cat# 50-5773-82; RRID: AB_11218868
PE anti-mouse GM-CSF, clone MP1-22E9	Biolegend	Cat# 505405; RRID: AB_315381
PE anti-mouse IL-4, clone 11B11	Biolegend	Cat# 504103; RRID: AB_315317
PE/Cy7 anti-mouse IL-10	Biolegend	Cat# 505025; RRID: AB_11149682
BV421 anti-mouse IL-17A, clone TC11-18H10	BD Biosciences	Cat# 563354; RRID: AB_2687547
PE anti-mouse IL-17F, clone eBio18F10	eBioscience	Cat# 12-7471-82; RRID: AB_1210742
PE/Cy7 anti-mouse IFN γ , clone AMG1.2	eBioscience	Cat# 25-7311-82; RRID: AB_469680
PE-CF594 anti-mouse ROR γ t, clone Q31-378	BD Biosciences	Cat# 562684; RRID: AB_2651150
BV510 anti-mouse TCR β , clone H57-597	BD Biosciences	Cat# 563221; RRID: AB_2738078
PE/Cy7 anti-mouse TNF α , clone MP6-XT22	eBioscience	Cat# 25-7321-82; RRID: AB_11042728
Mouse Fc Block (purified anti-CD16/32), clone 24G2	BD Biosciences	Cat# 553141; RRID: AB_394656
Bacterial and Virus Strains		
BL21(DE3) E.coli cells	New England Biolabs	Cat # C2527
Chemicals, Peptides, and Recombinant Proteins		
FITC-SMRT ID2 (FITC-NH-TNMGLEAIIRKALMGKYDQWEE)	LifeTein, LLC.	N/A
MOG 35-55 peptide	LifeTein, LLC.	LT12018, LT051716
Incomplete Freunds Adjuvant (IFA)	Fisher	Cat# PI-77145
Pertussis Toxin	List Biological Labs	Cat # 180
H27Ra TB	Difco	Cat# DF3114338
SR2211	Kumar et al., 2012	Dr. Ted Kamenecka
SR9009	Solt et al., 2011	Dr. Ted Kamenecka
Tween 80	Sigma-Aldrich	P8074
Kolliphor EL (Crempahor)	Sigma-Aldrich	C5135

(Continued on next page)

Continued

REAGENT or RESOURCE	SOURCE	IDENTIFIER
Phorbol 12-myristate 13-acetate (PMA)	Tocris	Cat # 1201
Ionomycin	Sigma-Aldrich	Cat # I0634
Lympholyte-M	Accurate Chemicals	Cat# ACL5035
Percoll	Sigma-Aldrich	Cat #P1644
TRIzol	Life Technologies	Cat# 10296-028
FuGene	Promega	Cat #E2311
Lipofectamine 3000	Invitrogen	Cat #L-3000008
Recombinant mouse IL-12	R & D Systems	Cat# 419-ML
Recombinant mouse IL-4	R & D Systems	Cat # 404-ML
Recombinant human TGF β	R & D Systems	Cat# 240-B
Recombinant mouse IL-6	R & D Systems	Cat# 406-ML
Recombinant mouse IL-23	R & D Systems	Cat# 1887-ML
Recombinant mouse IFN γ	R & D Systems	Cat# 485-MI-100
Recombinant mouse IL-1 β	R & D Systems	Cat# 410-ML
Recombinant mouse IL-21	R & D Systems	Cat# 594-ML
Xhol	NEB	Cat# R0146L
HpaI	NEB	Cat# R0105L
BamHI-HF	NEB	Cat# R3136L
HindIII-HF	NEB	Cat# R3104L
GolgiStop	BD Biosciences	Cat# 554724
RNase-free DNasel	Sigma-Aldrich	Cat# 4716728001
Liberase TL	Sigma-Aldrich	Cat# 5401020001
EDTA	Amresco	Cat# E177
DTT (Dithiothreitol)	Sigma-Aldrich	Cat# DTTR0
DMEM	Mediatech	Cat# 10-017-CV
IMDM	Life Technologies	Cat# 30980-097
L-glutamine	Life Technologies	Cat# 25030-081
Penicillin/streptomycin	Life Technologies	Cat# 15140-122
FBS	Gemini	Cat# 100-106
2-Mercaptoethanol	Sigma-Aldrich	Cat# M3148
Fixable viability dye eFluor 780	eBioscience	Cat# 65-0865-14
Fixable viability dye eFluor 506	eBioscience	Cat# 65-0866-14
6xHistag REV-ERB α LBD	Homemade	Dr. Doug Kojetin
6xHistag REV-ERB β LBD	Matta-Camacho et al., 2014.	Dr. Doug Kojetin
Polybrene	SantaCruz Biotechnology	Cat # sc-134220
Critical Commercial Assays		
EasySep mouse Naive CD4+ T cell isolation kit	StemCell Tech	Cat# 19765
RNeasy Plus Micro Kit	QIAGEN	Cat #74034
RNeasy Mini kit	QIAGEN	Cat # 74106
qScript cDNA synthesis Kit	QuantaBio/VWR	Cat #101414-100
PerfeCTa SYBR Green FastMix	QuantaBio/VWR	Cat# 101414-280
Dual-Glo Luciferase Assay System	Promega	Cat # E2940
Britelite Plus	Perkin Elmer	Cat #6066769
Amaxa EL4 Nucleofector kit	Lonza	Cat #VCA-1005
Zippy Plasmid Maxi Prep Kits	Zymo	Cat # D4028
QIAquick Gel extraction kit	QIAGEN	Cat# 28704
Pierce Coomassie (Bradford) Protein Assay kit	Thermo Fisher	Cat# 23200
TruSeq Stranded Total RNA Ribo-Zero Gold (H/M/R)	Illumina	Cat# RS-122-2301

(Continued on next page)

Continued

REAGENT or RESOURCE	SOURCE	IDENTIFIER
TruSeq Stranded Total RNA v2 with rRNA depletion	Illumina	Cat# RS-122-2001
SuperSignal West Femto Chemiluminescence	Thermo Fisher	Cat# PI34095
eBioscience Foxp3 Transcription Factor staining kit	Thermo Fisher	Cat # 00-5523-00
MOG 35-55/CFA Emulsion PTX (EAE induction kit)	Hooke Laboratories	EK-2110
PLP 139-151/CFA Emulsion PTX (EAE induction kit)	Hooke Laboratories	EK-2120
SimpleChIP Plus Sonication Chromatin IP kit	Cell Signaling Technology	Cat # 56383
Deposited Data		
REV-ERB overexpression RNA-seq	This paper	GEO: GSE122726
REV-ERB α WT versus KO RNA-seq	This paper	GEO: GSE122726
Experimental Models: Cell Lines		
HEK293 cells	ATCC	Cat# CRL-1573; RRID: CVCL_0045
PlatE cells	Cell Biolabs, Inc	Cat # RV-101
EL4 cells	ATCC	ATCC# TIB-39; RRID: CVCL_0255
Experimental Models: Organisms/Strains		
C57BL/6	Jackson Laboratories	Stock# 000664
SJL/J	Jackson Laboratories	Stock # 000686
KO (B6.Cg- <i>Nr1d1</i> ^{tm1Ven} /LazJ)	Jackson Laboratories	Stock # 018447; RRID: IMSR_JAX:018447
Rag1 ^{-/-} (B6.129S7- <i>Rag1</i> ^{tm1Mom} /J)	Jackson Laboratories	Stock # 003145
<i>Rorc</i> ^{f/f} (B6(Cg)- <i>Rorc</i> ^{tm3Litt} /J)	Jackson Laboratories	Stock # 008771
CD4 Cre (Tg(Cd4-cre)1Cwi/BfluJ)	Jackson Laboratories	Stock # 017336
Oligonucleotides		
Primers for qRT-PCR, see Table S3	This paper	N/A
ChIP primers <i>Il17a</i> promoter, see Table S3	Zhang et al., 2008	N/A
ChIP primers <i>Il17a</i> CNS2, see Table S3	Zhang et al., 2008	N/A
ChIP primers <i>Cry1</i> , see Table S3	This paper	N/A
ChIP primers <i>Nfil3</i> , see Table S3	Yu et al., 2013	N/A
ChIP primers <i>Rorc</i> , see Table S3	This paper	N/A
ChIP primers <i>Hprt</i> , see Table S3	This paper	N/A
Recombinant DNA		
MIGR1	Addgene	Addgene plasmid # 9044
MIGR1 REVERB α	Homemade	N/A
MIGR1 REVERB β	Homemade	N/A
MIGR1 REVERB α DBD	Homemade	N/A
MIGR1 REVERB α Δ DBD	Homemade	N/A
MIGR1 NFIL3	Homemade	N/A
pLMPd-Ametrine	Chen et al., 2014	Dr. Matthew Pipkin
shRNAmir: <i>Cd8a</i>	TransOMIC	Cat# TLMSU1400-12525
shRNAmir: <i>Nr1d2</i>	TransOMIC	Cat# TRMSU2000-353187
shRNAmir: <i>Nfil3</i>	TransOMIC	Cat# TRMSU2000-18030
MIGR1 ROR γ t	Addgene	Addgene plasmid #24069
pGL4 <i>ml17a-2kb</i> promoter+CNS5 luciferase	Zhang et al., 2008	Addgene plasmid # 20128
pGL3 <i>Bmal1</i> luciferase	Yu et al., 2002	Dr. Tom Burris
pGL4.73 Renilla	Promega	Cat# E691A
pcDNA3.1 REV-ERB α	Homemade	N/A
pcDNA3.1 REV-ERB α DBD	Homemade	N/A
pcDNA3.1 REVERB α Δ DBD	Homemade	N/A
pcDNA3.1 ROR γ t	Homemade	N/A
pCL-Eco packaging vector	Naviaux et al., 1996	Addgene plasmid #12371

(Continued on next page)

Continued

REAGENT or RESOURCE	SOURCE	IDENTIFIER
Software and Algorithms		
GraphPad Prism	GraphPad Software	https://www.graphpad.com
FlowJo (Version 10.4.1)	TreeStar	https://www.flowjo.com
R studio	R studio	N/A
DAVID	LHRI	https://david.ncifcrf.gov

CONTACT FOR REAGENT AND RESOURCE SHARING

Further information and requests for resources and reagents should be directed to and will be fulfilled by the Lead Contact, Laura Solt (lsolt@scripps.edu).

EXPERIMENTAL MODEL AND SUBJECT DETAILS**Animals**

The following mouse strains used were purchased from the Jackson Laboratory and/or were bred at Scripps Research – (Florida). C57BL/6J (B6); SJL/J, B6.Cg-Nr1d1^{tm1Ver}/LazJ (KO) (Chomez et al., 2000); B6.129S7-Rag1^{tm1Mom}/J (Rag1^{-/-}) (Mombaerts et al., 1992); B6(Cg)-Rorc^{tm3Litt/J} (Rorc^{fl/fl}) (Ivanov et al., 2006); Tg(Cd4-cre)1Cwi/BfluJ (CD4 Cre). Rorc^{fl/fl} mice were crossed with CD4 Cre mice to generate RORc^{fl/fl} x CD4 Cre mice. All experiments were conducted at controlled temperature (22–23°C), humidity ~60%, and 12h:12h light:dark cycles. Mice had access to regular chow (Harlan 2920X) and water, *ad libitum*. For all *in vitro* experiments, both male and female mice (8–10 weeks old) were sacrificed between 8 and 10am. For all *in vivo* experiments, 7–10 week-old male and female mice were used, and were sacrificed between 7 and 11am. For EAE experiments, mice were immunized between 11am and 1pm. The specific age and sex of the mice for experiments is described under each model's details below. All mice were maintained under specific pathogen free conditions. All studies conform to and were approved by the Institutional Animal Care and Use Committee (IACUC) at the Scripps Research Institute (Florida).

Cell lines

HEK293 (female), EL4 (unknown), and Plat-E (female) cells were cultured in DMEM supplemented with 10% FBS, 2mM L-glutamine, and 1% penicillin/streptomycin at 37°C, 5% CO₂ under standard culture conditions. Lymphocytes were cultured in IMDM medium with 10% FBS, 100IU/mL penicillin, 100 µg/ml streptomycin, 50µM β-mercaptoethanol, and 2mM L-glutamine. The gender of EL4 cells is unavailable at this time.

METHOD DETAILS**Chemical synthesis and reagents**

SR9009 has been previously described (Solt et al., 2012). Synthesis of SR12418 is as follows:

(S)-(3-((4-(tert-Butoxy)phenoxy)methyl)-6-fluoro-3,4-dihydroisoquinolin-2(1*H*)-yl)(naphthalen-1-yl)methanone

Step 1: (S)-3-carboxy-6-fluoro-1,2,3,4-tetrahydroisoquinolin-2-i um chloride

To a suspension of 3-fluoro-L-phenylalanine (10.0 g, 55.4 mmol) in conc. HCl (50 mL) was added aq. formaldehyde solution (37% wt.; 6.2 mL, 83.3 mmol). The reaction mixture was heated to 90°C and stirred for 5 h and the completion of the reaction was monitored by anal. HPLC. The mixture was then cooled to room temperature and filtered to give the title compound as the HCl salt (10.8 g, 84% yield), which was used without further purification. ¹H NMR (400 MHz, d-DMSO) δ 14.17 (broad S, 1H), 10.12 (broad S, 2H), 7.37-7.22 (m, 1H), 7.20-7.13 (m, 2H), 4.45-4.41 (m, 1H), 4.33 (m, 2H), 3.37 (dd, J = 16 Hz, 4.8Hz), 3.22-3.15 (m, 1H); ¹³C NMR (100 MHz, d-DMSO) 169.6, 161.1 (d, J = 242 Hz), 133.5 (d, J = 8.2 Hz), 128.6 (d, J = 8.4 Hz), 124.6 (J = 2.7 Hz), 115.0 (d, J = 21.8 Hz), 114.1(d, J = 21.8 Hz), 52.6, 43.2 and 28.0; ¹⁹F NMR (376.5 MHz, DMSO-d₆) δ -115.19, -119.13; MS (ESI) 196.1 (M + H).

Step 2: (S)-6-fluoro-3-(hydroxymethyl)-1,2,3,4-tetrahydroisoquinolin-2-i um chloride

BH₃.DMS (8.1 mL, 85.6 mmol) was added slowly to ((S)-3-carboxy-6-fluoro-1,2,3,4-tetrahydroisoquinolin-2-i um chloride (6.6 g, 28.5 mmol) and anhydrous THF (60 mL) at RT under argon. The mixture was then heated to 70°C for 3h monitoring the reaction by analytical HPLC. When the starting material was consumed, the reaction was cooled to RT and the reaction was quenched with THF/water (1:1) followed by dilute HCl (2M, 50 mL). The mixture was heated to 80°C for 3h and then cooled and concentrated to obtain the title compound as the HCl salt, which was used without further purification. ¹H NMR (400 MHz, d-DMSO) δ 9.88 (broad S, 1H), 9.61 (broad S, 1H), 7.36-7.32 (m, 1H), 7.15-7.10 (m, 2H), 5.61 (broad s, 1H), 4.27 (s, 2H), 3.84-3.68 (m, 2H), 3.51 (broad s, 1H), 3.0 (d, J = 8.0 Hz); ¹³C NMR (100 MHz, d-DMSO) 161.1 (d, J = 242 Hz), 134.4 (d, J = 8.1 Hz), 128.6 (d, J = 8.4 Hz), 125.0 (J = 2.8 Hz),

115.0 (d, $J = 21.3$ Hz), 113.7 (d, $J = 21.5$ Hz), 60.4, 53.8, 43.3 and 27.4; ^{19}F NMR (376.5 MHz, DMSO-d₆) δ –115.24, –119.22; MS (ESI) 182 (M + H).

Step 3: (S)-(6-Fluoro-3-(hydroxymethyl)-3,4-dihydroisoquinolin-2(1H)-yl)(naphthalen-1-yl)methanone

To a mixture of the above crude (S)-6-fluoro-3-(hydroxymethyl)-1,2,3,4-tetrahydroisoquinolin-2-iun chloride (28.5 mmol) in CH₂Cl₂ (100 mL) and NaHCO₃ (12 g, 142.6 mmol) was slowly added 1-naphthoyl chloride (4.71 mL, 31.4 mmol). The reaction was stirred at RT overnight. Water was added and the layers were separated. The aqueous layer was extracted with CH₂Cl₂ (2x150 mL). The combined organic layers were washed with brine, dried (Na₂SO₄), and concentrated. The resulting crude residue was purified by chromatography on silica gel (EtOAc/hexanes) to afford the title compound (6.94 g, 73% yield by 2 steps). ^1H NMR (400 MHz, d-DMSO) δ 8.06–6.88 (m, 10H), 5.52–5.10 (m, 1H), 4.44–2.77 (m, 7H); MS (ESI) 336 (M + H).

Step 4: (S)-(3-((tert-Butoxy)phenoxy)methyl)-6-fluoro-3,4-dihydroisoquinolin-2(1H)-yl)(naphthalen-1-yl)methanone

To the solution of (S)-(6-fluoro-3-(hydroxymethyl)-3,4-dihydroisoquinolin-2(1H)-yl)(naphthalen-1-yl)methanone (5.19 g, 15.5 mmol), 4-(tert-butoxy)phenol (2.83 g, 17.0 mmol) and n-Bu₃P (7.6 mL, 31.0 mmol) in anhydrous THF (100mL) under argon was added dropwise 1,1'-(azodicarbonyl)dipiperidine (ADDP) (7.8 g, 31.0 mmol) in anhydrous THF (70 mL). The reaction was stirred at RT overnight and the completion of the reaction was monitored by analytical HPLC. The precipitate was filtered and washed with hexane. The resulting filtrate was concentrated *in vacuo* to give the crude product which was purified by chromatography on silica gel (EtOAc/hex) to afford the title compound as a colorless solid (5.2 g, 69% yield); ^1H NMR (400 MHz, CDCl₃) δ 8.08–6.41 (m, 14H), 5.71–5.51 (m, 1H), 4.46–4.15 (m, 2H), 3.91–3.61 (m, 2H), 3.10–3.02 (m, 2H), 1.33–1.25 (m, 9H); ^{19}F NMR (376.5 MHz, CDCl₃) δ –114.88, –114.93, –115.55, –115.57; HRMS (ES+): m/z called for C₃₁H₃₀FNO₃ [M+H]: 484.2210; found 484.2294.

Induction and clinical evaluation of EAE

Chronic, MOG-induced EAE was induced in 10-week-old, female WT or KO mice by subcutaneous (s.c.) injections over two sites in the flank with 150 μ g per mouse of MOG_{35–55} peptide in an emulsion with CFA supplemented with 2.25 mg/ml *Mycobacterium tuberculosis*, strain H37Ra (500 μ g per mouse). Pertussis toxin was dissolved in PBS and injected i.p. at 200 ng per mouse 3 hr post immunization (Day 0) and 24 h later. For chronic, MOG-induced drug treatment experiments, 10-week-old, female B6 mice were immunized using EAE induction kits according to manufacturer's instructions. For R-EAE, 10-week old, female SJL/J mice were immunized using EAE induction kits according to manufacturer's instructions. Mice were scored daily on a scale of 0–5 in a double-blinded manner using the following criteria: 0, no clinical disease; 1, limp/flaccid tail; 2, limp tail and hind leg weakness; 3, limp tail and complete paralysis of hind limbs; 4, limp tail, complete hind limb and partial front limb paralysis; 5, quadriplegia or pre-moribund state. Gradations of 0.5 were used when mice exhibited signs that fell between two scores. For drug treatment experiments, SR12418 was dissolved in a 10% DMSO, 10% Tween 80, and 80% H₂O solution equaling 5mg/mL and administered intra-peritoneally (i.p.) at 50mg/kg as was vehicle control (10% DMSO, 10% Tween 80, and 80% H₂O) twice per day (b.i.d.). The treatment was started the evening of the immunization (MOG-EAE), or once the animals recovered from the first wave of disease (R-EAE) and continued for the duration of the experiment. For all b.i.d. dosing, animals were dosed at 7am and 7pm (lights on/lights off). At the termination of the experiment T cells were isolated from brain and spinal cord following perfusion of deeply anesthetized mice with cold PBS. CNS was minced before being passed through a 70um mesh cell strainer. Single cell suspensions were centrifuged and resuspended in 37% percoll. After further centrifugation, supernatant was removed and the pelleted mononuclear cells were washed and used for staining.

T cell-transfer colitis model

Spleens were collected from 8- to 10-week-old, female KO or control (WT) mice in order to sort naive CD4⁺ T cells. 5 \times 10⁵ CD4⁺CD25[−]CD62L^{hi}CD44^{lo} cells suspended in PBS were adoptively transferred i.p. (100 μ l/mouse) into 8-week-old, female Rag1^{−/−} recipient mice and monitored bi-weekly for body weight change. Beddings were routinely transferred between cages to distribute microflora and limit bias between cages regarding disease development. For drug treatment experiments, vehicle or SR12418 was administered starting at three-weeks post T cell transfer and continued for the duration of the experiment following procedures and time points described in the EAE experiments above. Mice were sacrificed to assess histological inflammation due to ethical requirements if they reached 80% or less of their original body weight. At the termination of the experiment, the whole colon and ileum (distal 1/3 part of the small intestine) were removed from the mouse. Colon length was measured first before each segment of the intestine was opened longitudinally and the fecal contents gently removed. Next, colon weights were measured prior to dissection longitudinally into two sections. One of the sections was rolled (Swiss roll) from the rectum along with the ileum and fixed in 10% neutral buffered formalin for 24 h. Swiss roll samples were then embedded in paraffin wax and sectioned for histological examination and immunohistochemistry staining. The other section of the colon was dissected in equal halves, designated as 'proximal' and 'distal' colon and snap frozen in dry ice for RNA analysis. *Histological Assessment of colon* - following overnight formalin fixation, paraffin-embedding, and standard H&E staining, histological colitis scoring of H&E-stained sections was performed blinded. Assessments of crypt architecture, crypt abscesses, tissue damage, goblet cell depletion, inflammatory cell infiltration, and neutrophil counts were assigned scores with the maximum combined score for each part of the intestine equaling 25 (Wang et al., 2015). For cell isolation - whole colons were removed, flushed with PBS to remove fecal contents, and opened longitudinally. Tissues were cut into small segments and incubated for 30 min at room temperature in DMEM without phenol red plus 0.15% DTT. After washing with media, intestines were incubated for 30 min at room temperature in media containing 1 mM EDTA to remove the epithelium. After

washing again with media, lamina propria was digested in media containing 0.25 mg/mL liberase TL and 10 U/mL RNase-free DNasel in a bacterial incubator for 15-25 min at 37°C. Single cell suspensions were passed through 70 µm mesh cell strainer and mononuclear cells were isolated by 70/30% percoll gradient centrifugation. Monocellular cells were washed two more times, counted, and used for FACS analysis.

Analysis of thymocytes

For the measurement of DP survival kinetics, male, 7-9 week-old, male C57BL/6 mice were treated with vehicle control or compounds for 3 days. All compounds were formulated in 15% cremophor at the following concentrations unless otherwise noted: SR2211 – 2mg/mL; SR9009 – 10mg/mL; SR12418 – 5mg/mL, and administered i.p., b.i.d. At the termination of the experiment, thymii were collected, minced, and passed through a 70um mesh cell strainer. Cell counts were performed prior to staining the cells for flow cytometry analysis.

In vitro CD4⁺ T cell differentiation

Naive CD4⁺ T cells from spleen and LNs of 8-10-week-old male and female mice were purified after removing the red blood cells using Lympholyte-M solution. Cells were enriched for naive CD4⁺ T cells using the mouse naive CD4⁺ T Cell Isolation Kit according to the manufacturer's instruction. If sorting was performed (FACS Aria II; BD Bioscience), the CD4⁺CD25⁺CD62L^{hi}CD44^{lo} fraction was collected. The conditions for the different T_H cell subsets were: For T_H0 (neutral conditions): 5 µg/ml anti-IL-4 and 5 µg/ml anti-IFN γ ; For T_H1 conditions: 5 µg/ml anti-IL-4, 20 ng/ml IL-12 and 10ng/ml IFN γ ; For T_H2 conditions: 5 µg/ml anti-IFN γ and 10ng/ml IL-4; For T_H17 conditions: 5 µg/ml anti-IFN γ , 5 µg/ml anti-IL-4, 1.5ng/ml TGF β and 30ng/ml IL-6; For iT_{reg} conditions: 5 µg/ml anti-IFN γ , 5 µg/ml anti-IL-4, and 5ng/ml TGF β . Other cytokines used for various T_H17 conditions: IL-1 β (10ng/ml), IL-21 (20ng/ml), and IL-23 (20ng/ml). 1×10^6 cells/ml of naive CD4⁺ T cells were activated with anti-CD3 and anti-CD28 by precoating plates with 100 µg/ml goat anti-hamster IgG. After 48 h, cells were removed from the TCR signal and recultured at a concentration of 1×10^6 cells/ml. Four days after activation, all cells were restimulated with 50ng/mL phorbol-12-myristate-13-acetate (PMA)and 1 µg/ml ionomycin for 2 hr with the addition of GolgiStop for an additional 2 hr before intracellular staining. Cells were cultured in IMDM medium with 10% FBS, 100IU/mL penicillin, 100 µg/ml streptomycin, 50uM β -mercaptoethanol, and 2mM L-glutamine. All cultures were performed in a volume of 200ul in 96-well U-bottomed plates.

Flow cytometry

Surface staining: single cell suspensions prepared from spleen, LNs, colons, CNS, etc. were washed and stained with fluorescence-conjugated antibodies for 20 min, washed, then resuspended in FACS buffer (0.5% BSA, 2mM EDTA in PBS). Intracellular cytokine staining: cells were re-stimulated with 50ng/mL PMA and 1 µg/ml ionomycin for 2 hr with the addition of GolgiStop for an additional 2 hr. Cells were then surface stained using procedures outlined above, fixed and permeabilized using the Foxp3 staining kit. Flow cytometric analysis was performed on a BD LSRII (BD Biosciences) instrument and analyzed using FlowJo software.

Retroviral Transduction

To generate murine REV-ERB α or REV-ERB β retroviral vectors, mouse REV-ERB sequences were inserted into the MIGR1 vector using the Xhol site and further screened for orientation. The DBD truncation construct was generated by PCR amplification of residues 103-225 of REV-ERB α with addition of 5' Xhol and 3' Hpal cut sites. The amplified product was cloned into the MIGR1 vector by double digest followed by T4 DNA ligation. The ΔDBD deletion construct was generated by a single PCR reaction of the MIGR1-REV-ERB α construct to delete residues 132-197. To generate the murine NFIL3 retroviral vector, the mouse NFIL3 sequence was inserted into the MIGR1 vector using the Xhol and BamHI sites. In each experiment, MIGR1 empty vector was used as a control. shRNAmirs against mouse CD8 (Cd8a) and Nfil3 were purchased from TransOMIC Technologies. shRNAmirs were PCR amplified and cloned into ametrine-expressing murine retroviral vectors (LMPd) containing the enhanced miR-30 cassette(Fellmann et al., 2013). MIGR1 ROR γ t retroviral construct was a gift from Dan Littman (Addgene Plasmid #24069). Virus production: Plat-E cells were cultured in DMEM containing 10% fetal bovine serum, 2mM L-glutamine, and 1% penicillin/streptomycin at 37°C under standard culture conditions. Plat-E cells were seeded at 350,000 cells/ml in a 6 well plate the day before transfection. 3 µg total retroviral plasmid DNA (1.5 µg MIGR1 plus 1.5 µg pCL-Eco) was transfected using Fugene6 reagent according to manufacturer's protocol. Viral supernatant was harvested 48 hr post transfection and used immediately for transduction. For retroviral transduction, naive CD4⁺ T cells were stimulated as indicated with anti-CD3 and anti-CD28 and cultured under T_H17 conditions. At 24 h post TCR priming, the culture medium was replaced with virus supplemented with 8 µg/ml polybrene. Plates were centrifuged at 1,800 rpm for 90 h at 37°C and then incubated at 37°C for 3-4 h. After this time, the medium was replaced with the original media removed before addition of virus.

Luciferase reporter assays

HEK293 cells were plated 24 hr prior to transfection in 96-well plates at a density of 15×10^3 cells/well. Transfections were performed using Lipofectamine 3000 according to manufacturer's protocol. To generate the DBD REV-ERB α truncation construct, residues 103-224 of the human REV-ERB α were cloned into the pcDNA3.1+ plasmid by HindIII and BamHI double digest. The ΔDBD deletion construct in was generated by PCR deletion of residues 131-197 of pcDNA3.1+ REV-ERB α . For drug treatments - 16 hr

post-transfection, cells were treated with vehicle or compound. 24 hr post-treatment luciferase activity was measured using BrightGlo and read using an Envision multilabel plate reader (PerkinElmer Life and Analytical Sciences). All values were normalized to DMSO to produce fold induction values. For assays in which drug treatment did not occur, luciferase activity was measured 24h post-transfection by DualGlo firefly and renilla luciferase reagents. Mouse EL4 cells were transfected using the Amaxa cell line nucleofector kit L according to manufacturer's instructions. 6 hr post-nucleofection, EL4 cells were stimulated with PMA (50ng/ml) and ionomycin (1ug/ml), plated in 12 well plates and incubated overnight for 16 hr. The following day, luciferase activity was measured as indicated for HEK293 cells. The pGL4 mll17a-2kb promoter + CNS5 was a gift from Warren Strober ([Zhang et al., 2008](#)). The pGL3 mBmal1 luciferase reporter has been previously described ([Solt et al., 2012; Yu et al., 2002](#)).

ChIP

ChIP assays were performed following manufacturer's instructions. Briefly, naive CD4⁺ T cells were differentiated under T_H17 conditions for 3 days, fixed in 1% formaldehyde for 10 min at room temperature, quenched in glycine (120mM) on ice for 5 min, and washed with PBS prior to lysis. Chromatin (20 x10⁶ cells/condition) was sheared with a Misonix S-4000 sonicator for 20 x 10 s cycles at 20% amplitude to yield 100-300 bp DNA fragments. After removing 1% as input DNA, immunoprecipitation was performed by adding anti-REV-ERB α antibody ([Cho et al., 2012](#)) (4ug/reaction) along with protein G magnetic beads on an end-to-end rotator at 4°C overnight. KO T_H17 cells and rabbit IgG were used as negative controls. Beads were then washed 3X with low salt ChIP buffer, followed by high salt ChIP buffer and eluted by re-suspending the beads in Elution Buffer. Both input and ChIP DNA were then incubated at 65°C for 30 min, followed by addition of Proteinase K and incubated at 65°C to reverse crosslink for 2 hr. DNA was then purified with QIAquick columns per manufacturer's instructions and resuspended in a 50 μ L volume. Real-time PCR detection of immunoprecipitated targets was performed using SYBR Green including passive reference dye (ROX) on a HT7900 Fast Real Time PCR system (Life Technologies, CA). A standard curve was generated for each sample based on amplification of serial dilutions of input DNA. ChIP DNA PCR reactions were performed in duplicates. Melt curves were analyzed to ensure amplification of specific target sequences. The primers used for qRT-PCR can be found in [Table S3](#).

Quantitative real-time PCR

For *in vitro* cultures, total RNA was extracted using a RNeasy Plus Micro Kit and reverse transcribed using iScript cDNA biosynthesis kit. Tissue samples (snap frozen and homogenized) – following isolation using TRIzol reagent mRNA was purified using RNeasy columns, followed by cDNA synthesis using iScript containing oligo (dT) and random hexamer primers. Real-time PCR was performed using SYBR Green including passive reference dye on a HT7900 Fast Real Time PCR system (Life Technologies, CA). All gene expression data were normalized to the housekeeping gene, β -actin unless otherwise mentioned, using a $\Delta\Delta$ cycle threshold-based algorithm followed by fold change comparison with the average of the control group. Primer efficiencies were determined using complementary DNA and primer dilutions for each gene of interest. Primers sequences for specific genes are provided in [Table S3](#).

RNA-sequencing and data analysis

mRNA was extracted from T_H17 cells on Day 2 (WT versus REV-ERB α KO cells) or Day 3 (MIGR1 transduced cells) of *in vitro* differentiation. Total RNA was extracted using QIAGEN RNeasy kits, quantified using the Qubit 2.0 Fluorometer (Invitrogen, Carlsbad, CA), and run on the Agilent 2100 Bioanalyzer (Agilent Technologies, Santa Clara, CA) for quality assessment. DNase-treated total RNA (300ng) was depleted of ribosomal RNA (rRNA) using appropriate probes provided by Illumina and further assessed on the bioanalyzer to confirm 18S and 28S rRNA peaks are depleted. rRNA-depleted RNA is processed using the TruSeq Stranded Total RNA sample prep kit. Briefly, RNA samples are chemically fragmented in a buffer containing divalent cations and heating at 94°C for 8 min. The fragmented RNA is random hexamer primed and reverse transcribed to generate first strand cDNA. The second strand is synthesized after removing the RNA template and incorporating dUTP in place of dTTP. cDNA is then end repaired and adenylated at their 3' ends. A corresponding 'T' nucleotide on the adaptors is utilized for ligating the adaptor sequences to the cDNA. The adaptor ligated DNA is purified using magnetic Ampure XP beads and PCR amplified using 12-13 cycles to generate the final libraries. The final libraries are size selected and purified using 1.0 x Ampure XP beads to remove any primer dimers. The final library size is typically 200-600bp with insert sizes ranging from 80-450bp. Final libraries are validated using bioanalyzer DNA chips and qPCR quantified using primers recognizing the Illumina adaptors. Libraries are pooled at equimolar ratios, quantified using qPCR (quantification of only the adaptor-ligated libraries) and loaded onto the NextSeq 500 flow cell at 1.8pM final concentration for pair end 75bp reads. 20-25 million mappable reads per sample were collected. Demultiplexed and quality filtered raw reads (fastq) generated from the NextSeq 500 were trimmed (adaptor sequences) using Flexbar 2.4 and aligned to the reference genome using TopHat version 2.0.9 ([Trapnell et al., 2009](#)). HT seq-count version 0.6.1 was used to generate gene counts and differential gene expression analysis was performed using Deseq2 ([Anders and Huber, 2010](#)). The normalized gene counts were used to plot the heatmaps using the heatmap package in R. To determine enriched functional groups in the RNA-seq data, KEGG pathway analysis was performed using DAVID ([Huang et al., 2009a; Huang et al., 2009b](#)).

TR-FRET corepressor interaction assay

The TR-FRET assay was performed in black low-volume 384-well plates (Greiner). Each well contained 4 nM 6xHistag-REV-ERB α LBD (human; residues 281–614) or 6xHistag-REV-ERB β LBD (human; residues 212–579) protein expressed in and purified from

Escherichia coli using nickel affinity and size exclusion chromatography; 1 nM LanthaScreen Elite Tb-anti-HIS Antibody; and 400 nM FITC-labeled peptide derived from the SMRT corepressor containing a N-terminal FITC label with a six-carbon linker (Ahx) and an amidated C terminus for stability in TR-FRET buffer (20 mM potassium phosphate, pH 7.4, 50 mM potassium chloride, 1 mM dithio-threitol, and 0.005% Tween-20). Ligand stocks were prepared via serial dilution in DMSO, added to wells in triplicate, and plates were incubated at 4°C for 2 h and read using BioTek Synergy Neo multimode plate reader. The Tb donor was excited at 340 nm; its fluorescence emission was monitored at 495 nm, and the acceptor FITC emission was measured at 520 nm; and the TR-FRET ratio was calculated as the signal at 520 nm divided by the signal at 495 nm. Data were plotted using GraphPad Prism as TR-FRET ratio versus ligand concentration and fit to sigmoidal dose response curve equation.

Immunoblot Analysis

T cells were washed once with phosphate-buffered saline and then incubated for 10 min at 4°C in 100 µL of TNT lysis buffer (50 mM Tris-Cl, pH 7.5, 150 mM NaCl, and 1% Triton X-100) containing protease inhibitors. Samples were then vortexed for 30 s and centrifuged (14,000RPM for 10 min). Protein levels in the supernatants were determined using a Coomassie protein assay kit, and 15 µg of protein from each sample was separated by SDS-PAGE (10%) and transferred to a PVDF membrane and immunoblotted with primary antibodies: mouse ROR γ t and Actin. KLH-conjugated (LifeTein, LLC.) peptides were designed to generate paralog-specific antibodies recognizing epitopes spanning amino acid residues 268 to 279 of REV-ERB α and were injected in rabbits, similar to what has been previously described (Cho et al., 2012). Peptides were synthesized by LifeTein, LLC. (Somerset, NJ, USA). Immunization and serum collection were performed by Pocono Rabbit Farm and Laboratories (Canadensis, PA), and antibodies were purified by peptide affinity chromatography. Horseradish peroxidase-conjugated secondary antibodies were purchased from Jackson ImmunoResearch. Detection of the bound antibody by enhanced chemiluminescence was performed according to the manufacturer's instructions.

QUANTIFICATION AND STATISTICAL ANALYSIS

All data are expressed as the mean ± SEM. All statistical analyses were performed using GraphPad PRISM 6. Student's t test was used for comparison between two groups. To compare differences between groups *in vivo*, a 2-way ANOVA with Bonferroni's multiple comparison test was performed if values were derived from a normal distribution. Where a normal distribution could not be confirmed or sample size was small, nonparametric Mann-Whitney U tests with a post hoc test were performed. A *p* value of < 0.05 was considered statistically significant. The number of sample replicates and statistical cut-offs used in the analysis of genomics data are indicated in the figure legends or the text.

DATA AND SOFTWARE AVAILABILITY

All next-generation sequencing data generated for this paper were deposited in the Gene Expression Omnibus (GEO) under accession number GEO: GSE122726.

Supplemental Information

REV-ERB α Regulates

T_H17 Cell Development and Autoimmunity

Mohammed Amir, Sweena Chaudhari, Ran Wang, Sean Campbell, Sarah A. Mosure, Laura B. Chopp, Qun Lu, Jinsai Shang, Oliver B. Pelletier, Yuanjun He, Christelle Doebelin, Michael D. Cameron, Douglas J. Kojetin, Theodore M. Kamenecka, and Laura A. Solt

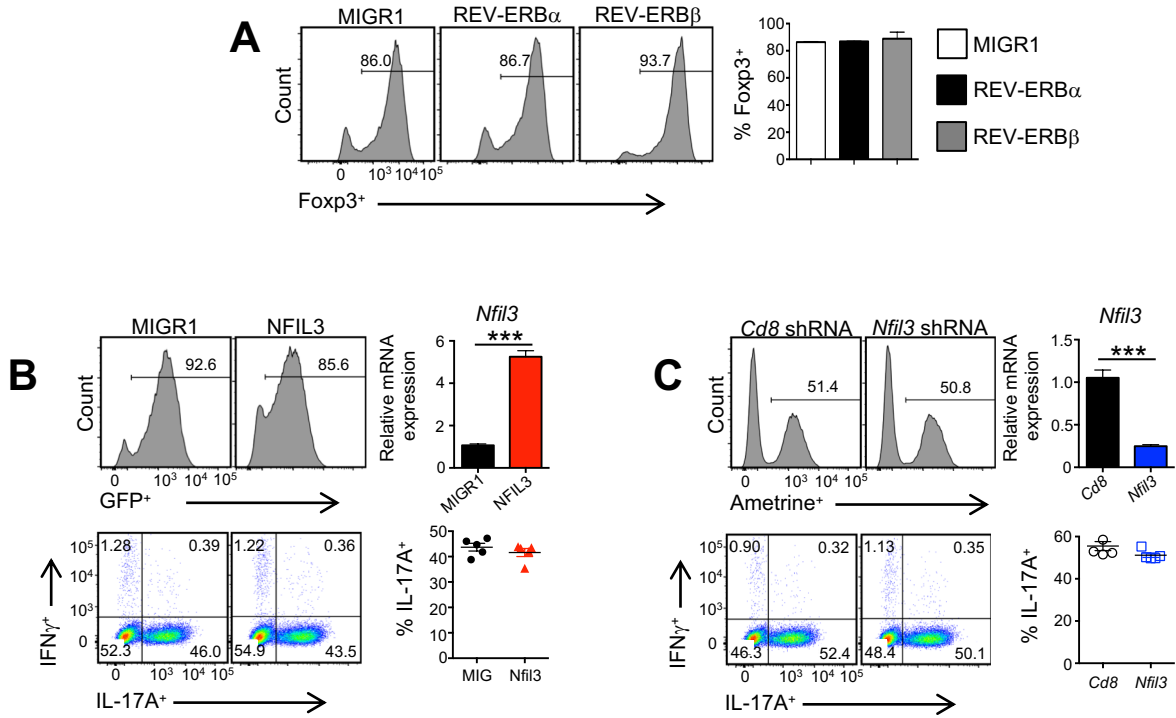


Figure S1. Overexpression of the REV-ERBs does not affect iTreg development. Related to Figure 1. (A) FACS analysis of Foxp3 expression in CD4⁺ T cells activated under iTreg polarizing conditions and transduced with MIGR1, REV-ERB α , and REV-ERB β retroviral vectors. Graph (right) represents % Foxp3 cells in the culture. (n=3) (B) FACS analysis of CD4⁺ T cells activated under Th17 polarizing conditions and transduced with MIGR1 or MIGR1 NFIL3 retroviral vectors. FACS plots (top) represents % GFP⁺ cells in the culture. Graph (top right) is relative mRNA expression of *Nfil3* in sorted live, GFP⁺ cells. β -actin was used as the internal control. FACS plots (bottom) represent % IL-17A⁺ cells in live GFP⁺ gates. Graph (bottom right) represents % IL-17A⁺ cells in live, GFP⁺ gates from several experiments. (n=5) (C) FACS analysis of CD4⁺ T cells activated under Th17 polarizing conditions and transduced with control shRNA (Cd8) or *Nfil3* shRNA retroviral vectors. FACS plots (top) represents % Ametrine⁺ cells in the culture. Graph (top right) is relative mRNA expression of *Nfil3* in sorted live, Ametrine⁺ cells. β -actin was used as the internal control. FACS plots (bottom) represent % IL-17A⁺ cells in live, Ametrine⁺ gates. Graph (bottom right) represents % IL-17A⁺ cells in live, Ametrine⁺ gates from several experiments (n=4). Data represent mean \pm s.e.m. *p<0.05, ns, not significant (p>0.05).

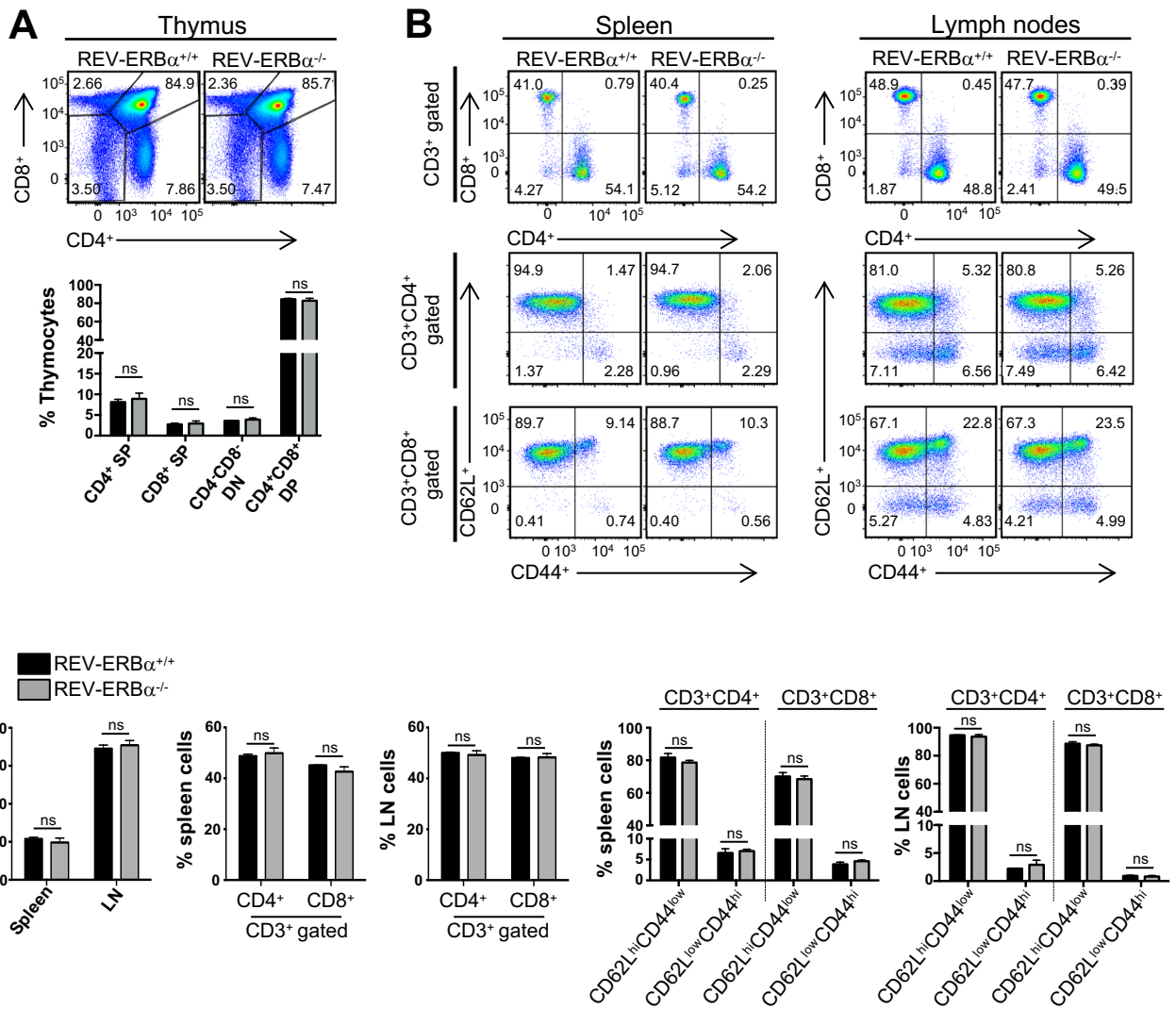


Figure S2. Characterization of REV-ERB α KO mice. Related to Figure 2. (A) FACS analysis of thymocytes from 8-week old REV-ERB $\alpha^{+/+}$ (WT) or REV-ERB $\alpha^{-/-}$ (KO) mice stained with anti-CD4 and anti-CD8 antibodies. Graph (below) depicts the frequency of thymocytes per subset. (SP – single positive; DP – double positive; DN – double negative) (B) (top panels) FACS analysis of CD3⁺CD4⁺ or CD3⁺CD8⁺ T cells in the spleen and lymph nodes of REV-ERB $\alpha^{+/+}$ or REV-ERB $\alpha^{-/-}$ mice. (bottom panels) FACS analysis of naïve (CD62L^{high}CD44^{low}) and effector T cell (CD62L^{low}CD44^{high}) populations from the spleen and lymph nodes of REV-ERB $\alpha^{+/+}$ or REV-ERB $\alpha^{-/-}$ mice. (C) Graphs depicting the frequencies of T cells and their subsets in the spleens and lymph nodes of REV-ERB $\alpha^{+/+}$ or REV-ERB $\alpha^{-/-}$ mice shown in Panel B. Data represent mean \pm s.e.m. (n=3/group). *p<0.05, ns, not significant (p>0.05).

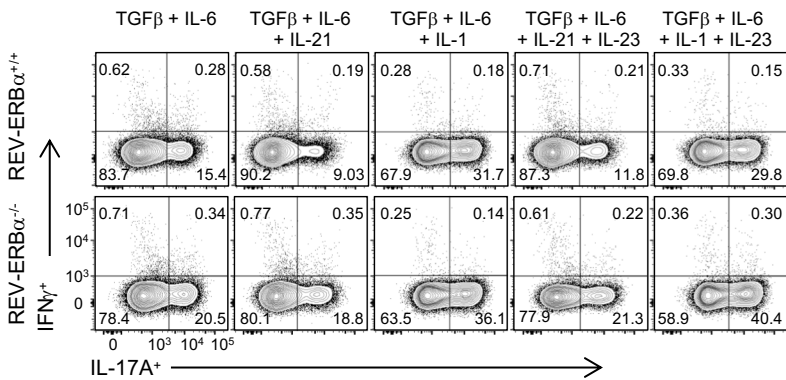
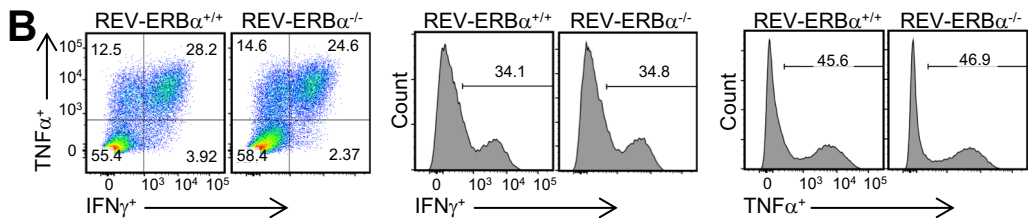
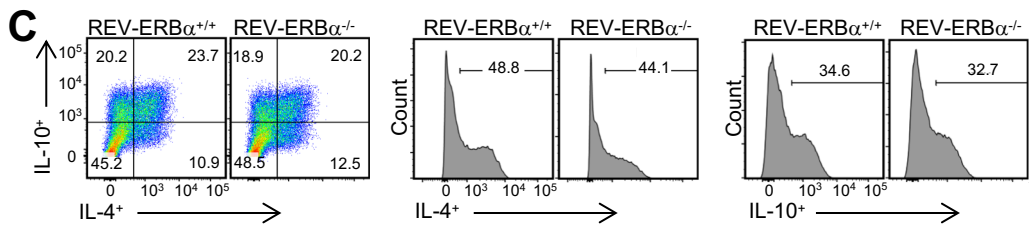
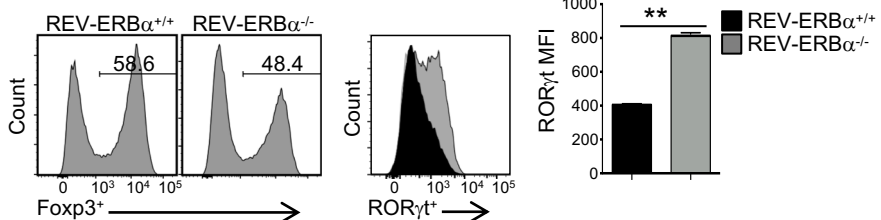
A**B****C****D**

Figure S3. Loss of REV-ERB α affects T_H17 cells but has no effect on T_H1 and T_H2 cells *in vitro*. Related to Figure 2.
(A) FACS analysis of IL-17A and IFN γ expression from different T_H17-cell culture conditions from REV-ERB $\alpha^{+/+}$ or REV-ERB $\alpha^{-/-}$ mice. (n=4) **(B and C)** FACS analysis of naïve CD4 $^{+/-}$ T cells differentiated into T_H1 or T_H2 cells, respectively, from REV-ERB $\alpha^{+/+}$ or REV-ERB $\alpha^{-/-}$ mice. **(D)** FACS analysis of Foxp3 (left) or ROR γ t (right) expression from naïve CD4 $^{+/-}$ T cells differentiated under iTreg-polarizing conditions from REV-ERB $\alpha^{+/+}$ and REV-ERB $\alpha^{-/-}$ mice. Graph indicates MFI of ROR γ t expression in the FACS plots. (n=2, repeated 3 times) **p<0.01, determined using Student's t-test.

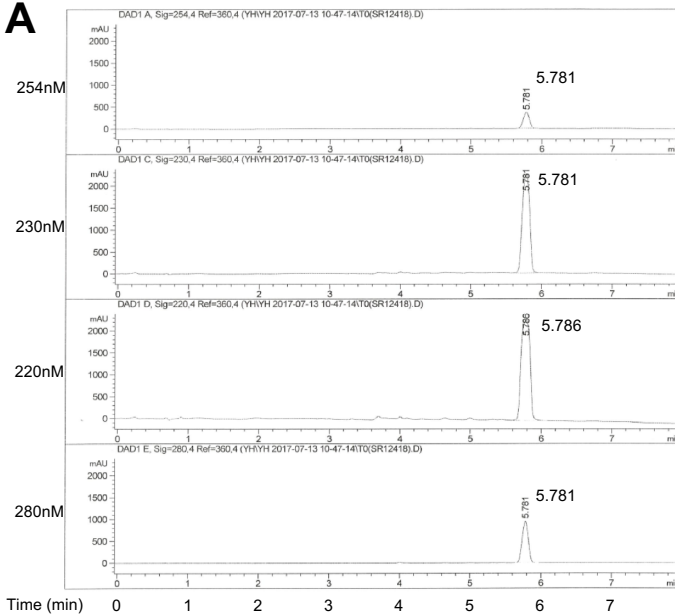
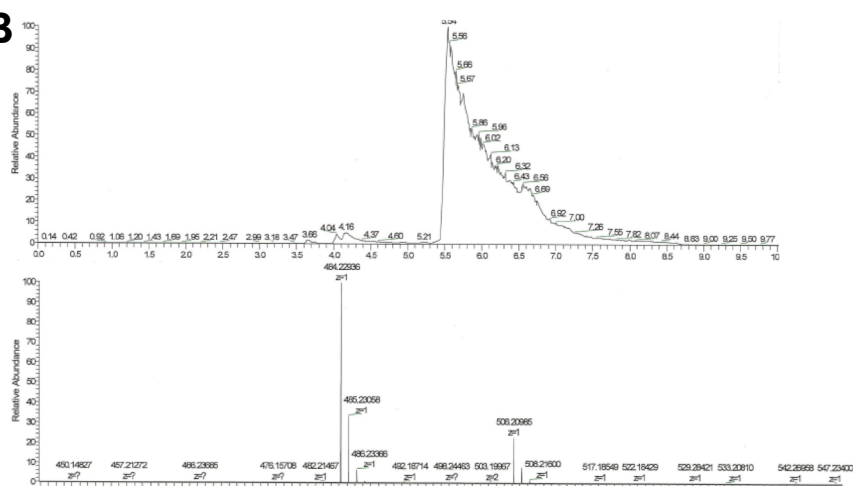
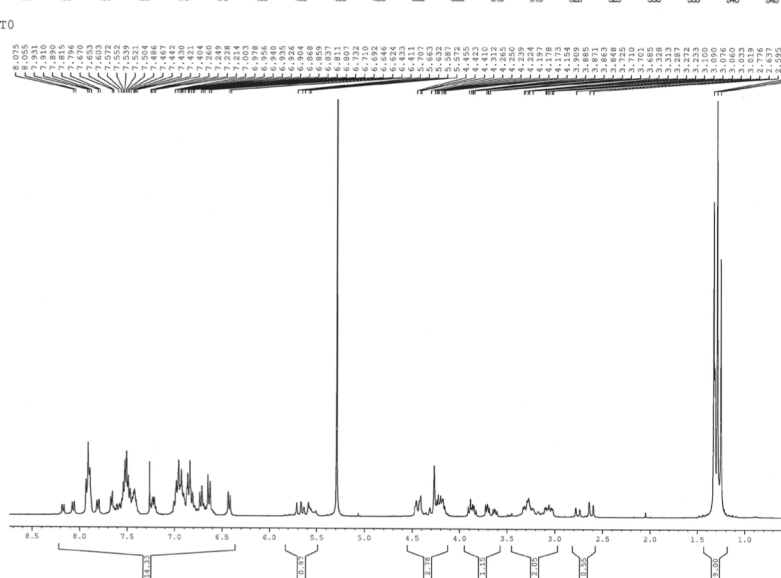
A**B****C**

Figure S4. Characterization of SR12418. Related to Figure 5. (A) Sample purity of SR12418 by reverse phase analytical HPLC. Four traces indicate data collected at distinct wavelengths (220, 230, 254, and 280nM). (B) Mass spectral analysis of SR12418. (C) ¹H-NMR analysis of SR12418.

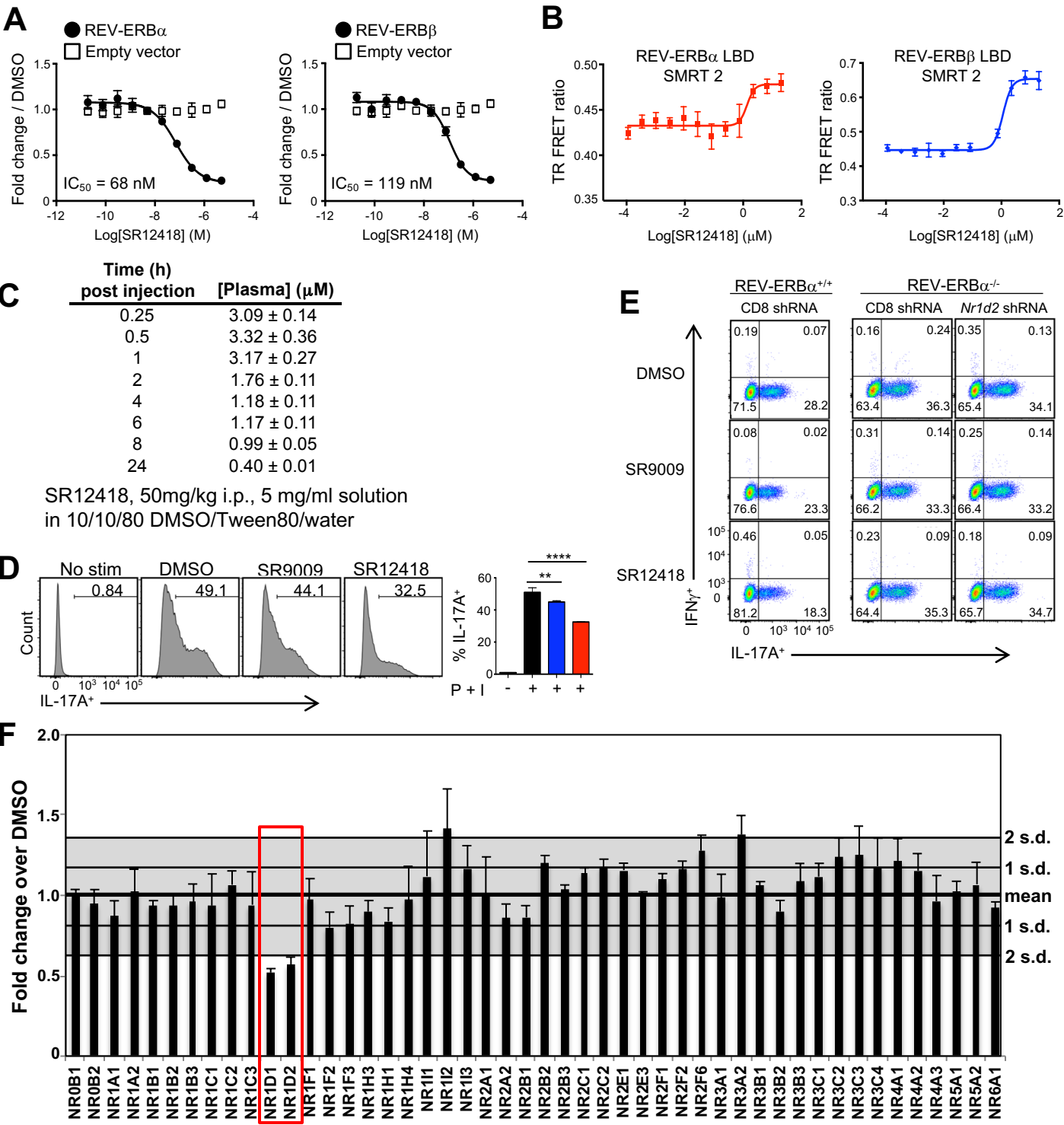


Figure S5. Specificity and effects of SR9009 and SR12418 on T_H17 cell development. Related to Figure 5. (A) Cotransfection assay in HEK293 cells using REV-ERB α and REV-ERB β and a luciferase reporter driven by the *Bmal1* promoter. Graphs demonstrate SR12418 dose-dependently suppressed *Bmal1* luciferase activity. (n=4) (B) TR-FRET biochemical data performed with REV-ERB α and REV-ERB β LBD indicating that SR12418 binds to each receptor causing recruitment of corepressor SMRT ID2 peptide. (n=3) (C) Pharmacokinetic analysis of SR12418 in mice. Data represents mean \pm s.e.m. (n=3) (D) FACS of IL-17A expression in EL4 cells +/- PMA and Ionoycin (P+I) treatment for 16h in the presence of Vehicle or REV-ERB ligands (5 μ M). (n=3) (E) Specificity of SR9009 (5 μ M) and SR12418 (5 μ M) was assessed in T_H17 cells from WT and REV-ERB $\alpha^{-/-}$ mice transduced with *Cd8* shRNA or shRNA to REV-ERB β (*Nr1d2*). Drugs were added after 48h post T-cell activation. FACS analysis was performed 96h post T-cell activation. (n=3) (F) Nuclear receptor specificity assay illustrating the activity of SR12418. All 48 human nuclear receptors are represented in this cotransfection assay. SR12418 was tested at a concentration of 20 μ M. HEK293 cells were transfected with GAL4 DNA binding domain – nuclear receptor fusion constructs. (n=4) Data represents mean \pm s.e.m. ** p < 0.01, ***p < 0.001.

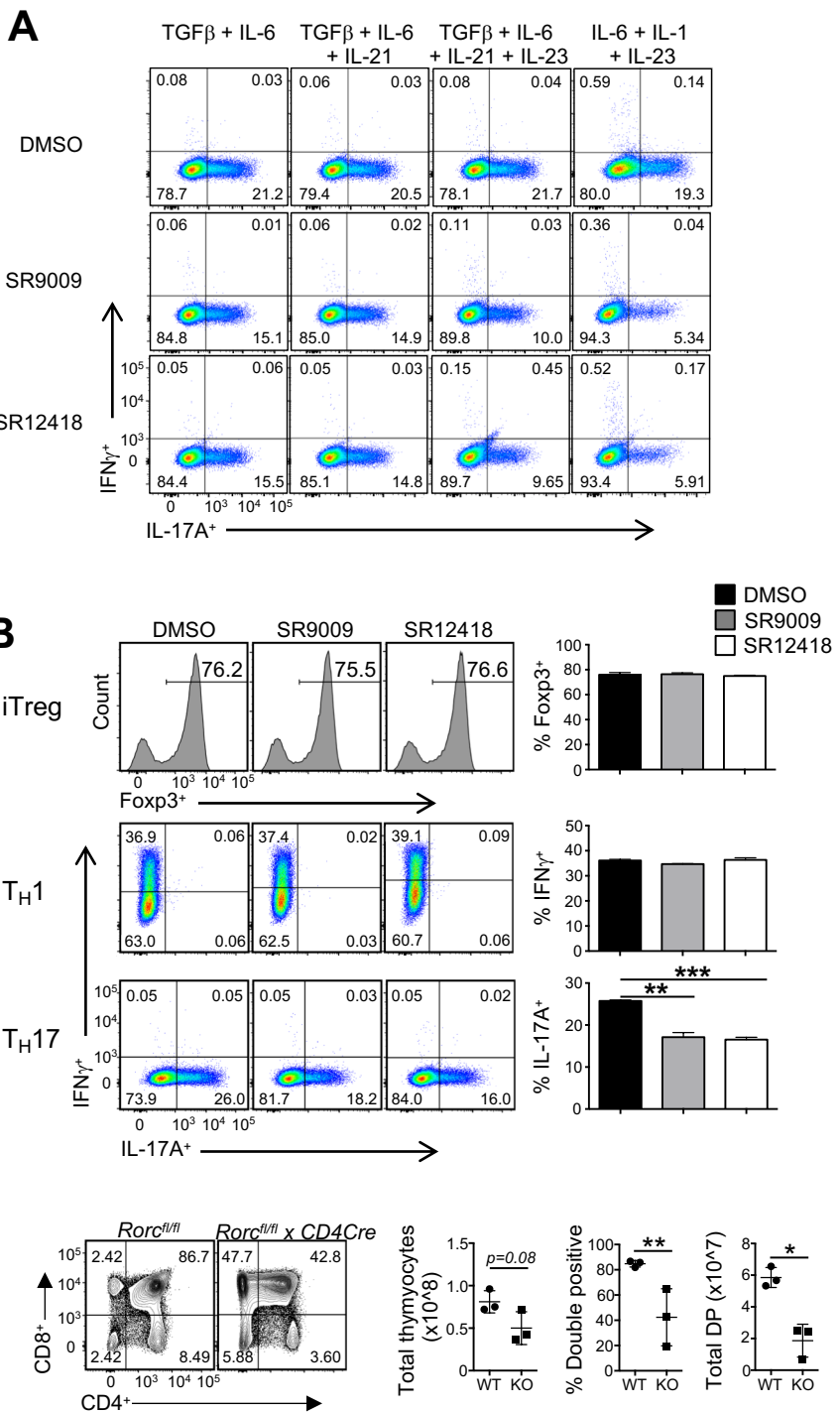


Figure S6. REV-ERBα-specific small molecules suppress T_H17-cell development and function. Related to Figure 5. (A) FACS analysis of IL-17A and IFN γ expression from different T_H17-cell culture conditions in the presence of vehicle (DMSO), SR9009 (5 μ M), or SR12418 (5 μ M). (n=3) (B) FACS analysis and graphs depicting percent Foxp3⁺ cells in iTreg cultures (top), IL-17A and IFN γ expression from T_H1 (middle) and T_H17 (bottom) cell culture conditions in the presence of vehicle (DMSO), SR9009 (5 μ M), or SR12418 (5 μ M). (n=3) (C) FACS analysis of thymocytes from *Rorc*^{fl/fl} and *Rorc*^{fl/fl} x CD4 Cre mice. Graphs depict quantification of total thymocyte number, double positive percentage, and double positive number in each group. Data shown are representative of two separate, independent experiments (n=3/group). Data represents mean \pm s.e.m. ** $p<0.01$, *** $p<0.001$ determined using Student's t-test.

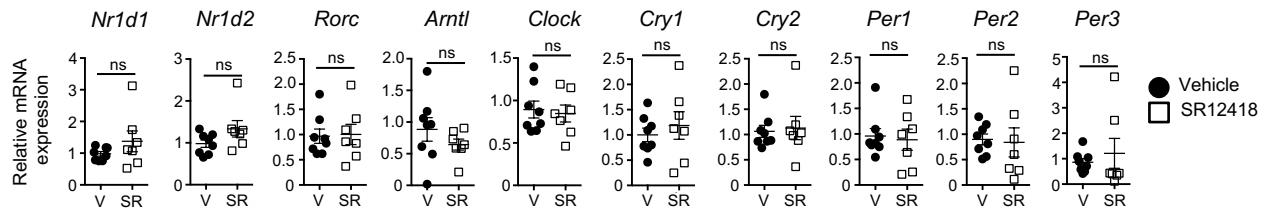
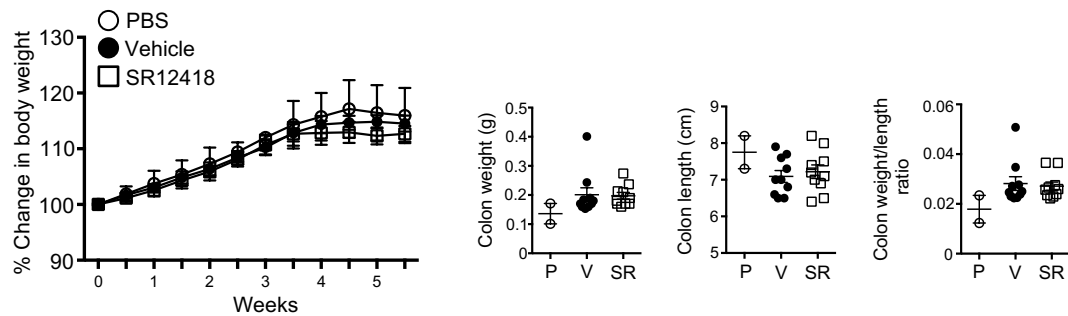
A**B**

Figure S7. SR12418 does not perturb the circadian rhythm or affect body/colon weight in colitis. Related to Figures 6 and 7. **(A)** qRT-PCR analysis of livers from EAE mice from Figure 6. mRNA is normalized to *18s*. (*Arntl*, *Bmal1*) (n= 8, V; 7, SR). **(B)** Percent change in body weight, colon weights, colon lengths, and colon weight/length ratios of *Rag1^{-/-}* recipient mice over 6 weeks post-adoptive transfer of WT T cells. SR12418 and vehicle treatment began at 3 weeks post-transfer. V= vehicle; SR = SR12418; P = PBS control (no cells). Data are mean±s.e.m. (n=10/group; PBS, n=2). ns, not significant determined using Student's *t*-test.

Table S1. List of differentially expressed genes between groups from REV-ERB overexpression RNA-sequencing studies. Related to Figure 1.

Adam19	Il12rb1	Evl	Rora
Il17f	Gm42418	Tgfb3	Adam8
Furin	Myo3b	Khl6	Myadm
Tecpr1	Myo10	Arap2	Gm37194
Il17a	Fgl2	Lnpep	Cysltr1
Gbp2	Rbpj	Igfbp4	Scml4
Smox	Arl4c	Tbl1xr1	Ccr5
Ahr	Cndp2	Ptger4	Ehd4
Ppp1r14c	Cpox	Nos2	Cnot6
Plin2	Abcg3	Sema4f	H2afy
Serpinb5	Itga4	Nrip1	Sipa1l1
Nr1d1	Lbp	Aebp2	Arhgef3
Gcnt2	Arhgap39	Slfn1	Hic1
Ltb4r1	Cdh17	Myo1f	Cd3g
Dgat1	Cysltr2	Plcl2	Treml2
Sell	Nrn1	S1pr3	Leo1
Itga3	Cyp1b1	Il17ra	
Gbp7	Gbp3	Tgm1	
Iyd	Cry1	Elk4	
Neb1	Txk	Sesn3	
Neb	Id2	Cd27	
Aff3	Frmd6	Mthfd1l	
Btla	Jak2	Wbp1l	
Fes	Sepp1	Aco2	
Pim1	Tex2	Il2rb	
Tnk2	Cpd	Klh124	
Plac8	Gbp9	Gpld1	
Ncf1	Lilrb4a	Iqgap2	
Rgs1	Cd5	Npas2	
Stab1	Il12rb2	Gbp6	
Enpp2	Ipcef1	Slamf6	
Gcnt1	Casr	Ccdc63	
Trpm6	Disp1	Pdcd4	
Il22	Gbp8	B3galt2	
Gzmb	Gimap4	Ttc39c	
Gpr15	Atp10a	Pkhd1l1	
Il23r	Arntl	Nt5e	
Slfn2	St6gal1	Ppp1r3b	
Gm26917	Lef1	Por	
Gbp4	Tcf7	Lilr4b	
Slc15a3	Mapk14	Dusp4	
Wdr1	Pak1ip1	Arl5a	
Atp2b4	5430421N21Rik	Grn	
Cldnd1	Stat4	Cd9	
Chd3	Bcl2l11	Tgm2	
Nfil3	Klf13	Serpine1	
Ccl20	Mctp2	Il10	
Ptpn13	Dennd5a	Cd28	
Lrrkip1	Osbpl9	Igf2r	

Table S2. List of differentially expressed genes between groups from WT versus REV-ERB α knock out RNA-sequencing studies. Related to Figure 2.

Sifn2	Pctp	Nos2
Xist	Mtmar7	Gpr146
Alpk2	Timd2	Pbdc1
Eif2s3y	Dntt	Sifn8
Basp1	Rdm1	Kcnq1ot1
Igfbp4	Anxa3	Me2
Kdm5d	Chchd10	Arl4c
Ddx3y	Irf8	Wfikkn2
Eif2s3x	Ncf1	Slc11a2
Il9	Cyp11a1	Traip
Uty	Ccl20	Sema7a
Il24	Msi2	Lipe
Thra	1700048O20Rik	Gm10801
Lta	H2-Q7	Mmd
Izumo1r	Rnu3a	C030037D09Rik
Jak3	H2-Q10	Coro2a
Il17a	Eno3	Nebl
Igf2bp3	Rnf157	Taf15
Kdm5c	Myb	Fes
Kdm6a	Tmem176b	Rgcc
AA465934	Sifn1	Il7r
Glod4	Socs1	Nme1
Tlcd2	Rcn1	Ubtd1
Slc43a2	Slamf1	Cd24a
Chd3	Gatm	Sdcbp2
Rsad1	Tgm1	Tbc1d4
Il2	App	Cyp51
H2-Q6	Pcx	Mt2
Bzrap1	Scarna2	Socs3
Socs2	Pim1	Procr
Gpr83	Tfrc	
Tnfsf11	Ccdc50	
PISD	She	
Il17f	Gm23849	
Yap1	Lbp	
Itpripl2	2610035D17Rik	
Gm26917	Acvrl1	
Znrf2	Hemk1	
Adam19	Aldh1l1	
Tgm2	Tmem176a	

Table S3. List of primers used in this study for qRT-PCR or ChIP analysis. Related to Star Methods: Quantitative real-time PCR and Chromatin Immunoprecipitation

Gene name	Forward primer (5' - 3')	Reverse Primer (5' - 3')
<i>Arntl</i>	CAGGCTAGCTTGATAGGACAGA	CCAGTGTAGGGGTGACTGTAAAC
<i>b-actin</i>	CCACAGCTGAGAGGGAAATC	AAGGAAGGCTGGAAAAGAGC
<i>18s</i>	GTAACCCGTTGAACCCCATT	CCATCCAATCGGTAGTAGCG
<i>Clock</i>	AGAACCTGGCATTGAAGAGCTC	GTCAGACCCAGAATCTGGCT
<i>Cry1</i>	CACTGGTCCGAAAGGGACTC	CTGAAGCAAAATGCCACCT
<i>Cry2</i>	CACTGGTCCGCAAAGGACTA	CCACGGGTCGAGGATGTAGA
<i>Cxcl2</i>	ACGTGTTCCAGGACACAACA	ACAAACCCCTCCCCACCTAAC
<i>Cxcl10</i>	TCCTTGTCCCTCCCTAGCTCA	ATAACCCCTGGGAAGATGG
<i>Foxp3</i>	GAGCCAGAAGAGTTCTCAAGC	CATAGCTCCCAGCTTCTCCTT
<i>Gata3</i>	TCTCAC TCTCGAGGCAGCATGA	GGTACCATCTCGCCGCCACAG
<i>Ifng</i>	TGGCTTTCTGGCTGTTACT	GCTCTGCAGGATTTCATGTC
<i>Il1b</i>	GTTCCTCCTTGCCTCTGA	GCTGCCTAATGTCCCCTT
<i>Il6</i>	CATGTTCTCTGGAAAATCGTG	TCCAGTTGGTAGCATCCATC
<i>Il17a</i>	CTCCAGAAGGCCCTCAGACTAC	AGCTTCCCTCCGCATTGACACAG
<i>Il17f</i>	GAGGATAACACTGTGAGAGTTGAC	GAGTCATGGTGCTGTCTTC
<i>Il22</i>	TCA TCG GGG AGA AAC TGT TC	CAT GTA GGG CTG GAA CCT GT
<i>Il23r</i>	TGTGGATCCTGTCCCTACAGAG	CCTAGAGGACAGTCTTGTCTCA
<i>Nfil3</i>	CTTCAGGACTACCAGACATCCAA	GATGCAACTCCGGCTACCA
<i>Nr1d1</i>	ACCTTGAGGTGCTGATGGT	CTCGCTGAAGTCAAACATGG
<i>Nr1d2</i>	TGTAAAACAGGCCAAACCCA	CCCTTACAGCCTTCACAAGC
<i>Per1</i>	CGGATTGCTATATTCGGAGCA	TGGGCAGTCGAGATGGTGT
<i>Per2</i>	AGCGCAAGGTCCGAGTTAG	GCTGCAACTGGAAATATGAAGC
<i>Per3</i>	AACACGAAGACCGAAACAGAAT	CTCGGCTGGAAATACTTTTCA
<i>Rora</i>	AACCCGAACCCATATGTGAC	ATGTTCTGGGCAAGGTGTC
<i>Rorc</i>	CCGCTGAGAGGGCTTCAC	TGCAGGAGTAGGCCACATTACA
<i>Tnfa</i>	TCAGCCGATTGCTATCTCAT	TGGAAGACTCCTCCCAGGTAT
ChIP primers	Forward primer	Reverse Primer
<i>Il17a</i> promoter	GCAGCAGCTTCAGATATGTCC	GGGGTGACACCATTGAGTAA
<i>Il17a</i> CNS2	CCGTTAGACTGAAACCCAGTC	GTACCTATGTGTTAGGAGGCGC
<i>Cry1</i>	GTCTCTAGGGTCGACACTGTATGGTT	AGTGGGTGGTTAGCATACTCCCAC
<i>Nfil3</i>	GCGATGAAACGTGGGCACCG	CGTCACAATGGCTCGTCCGGG
<i>Rorc</i>	TCCAGCCAGAAGATGAAGGT	AAGTCTGGCAGGAGGAACAA
<i>Hprt</i>	CCTAAATCTTGAGGAATCACATCA	TTCTTCTGAAGAAAATGGTACTGG